Acclimation of oxygenic photosynthesis to iron starvation is controlled by the sRNA IsaR1

Jens Georg[1], Gergana Kostova[1], Linda Vuorijoki[2], Verena Schön[1#], Taro Kadowaki[3], Tuomas Huokko[2], Desiree Baumgartner[1], Maximilian Müller[1†], Stephan Klähn[1], Yagut Allahverdiyeva[2], Yukako Hihara[3], Matthias E. Futschik[4,§], Eva-Mari Aro[2], Wolfgang R. Hess[1*]

CURRENT-BIOLOGY-D-17-00165R1
in press, April 10, 2017

[1]Genetics & Experimental Bioinformatics, Institute of Biology III, Faculty of Biology, University of Freiburg, Schänzlestr. 1, 79104 Freiburg, Germany;

[2]Molecular Plant Biology, Department of Biochemistry, University of Turku, 20014 Turku, Finland;

[3]Graduate School of Science and Engineering, Saitama University, Saitama 338-8570, Japan;

[4]CCMAR - Center of Marine Sciences, University of Algarve, Campus de Gambelas, 8005-139 Faro, Portugal

Current addresses:

[#]University of Vienna, Department of Ecogenomics and Systems Biology, Althanstraße 14, 1090 Vienna, Austria;

[†]Institute for Cell and Gene Therapy, University of Freiburg, Breisacher Str. 115,·79106 Freiburg, Germany

[§]School of Biomedical and Healthcare Sciences, Plymouth University, Plymouth, UK

***Lead contact / Corresponding author:** Wolfgang R. Hess; Phone: +49-761-203-2796; Fax: +49-761-203-2745; Email: Wolfgang.Hess@biologie.uni-freiburg.de

Running title: Regulation by the cyanobacterial sRNA IsaR1

Summary

Oxygenic photosynthesis crucially depends on proteins that possess Fe^{2+} or Fe/S complexes as co-factors or prosthetic groups. Here, we show that the regulatory sRNA IsaR1 (Iron-stress activated RNA 1) plays a pivotal role in acclimation to low iron conditions. The IsaR1 regulon consists of more than 15 direct targets including Fe^{2+}-containing proteins involved in photosynthetic electron transfer, detoxification of anion radicals, citrate cycle, and tetrapyrrole biogenesis. IsaR1 is essential for maintaining physiological levels of Fe/S cluster biogenesis proteins during iron deprivation. Consequently, IsaR1 affects the acclimation of the photosynthetic apparatus to iron starvation at three levels: (i) directly, via posttranscriptional repression of gene expression, (ii) indirectly, via suppression of pigment and (iii) Fe/S cluster biosynthesis. Homologs of IsaR1 are widely conserved throughout the cyanobacterial phylum. We conclude that IsaR1 is a critically important riboregulator. These findings provide a new perspective for understanding the regulation of iron homeostasis in photosynthetic organisms.

Key words: cytochrome b_6f complex, electron transfer, Fe/S cluster biogenesis, ferredoxin I, iron homeostasis, photosynthesis, regulatory sRNA, *Synechocystis*

INTRODUCTION

Oxygenic photosynthesis requires iron cofactors, e.g., in its electron transfer systems, within the numerous Fe/S cluster-containing proteins and particularly in photosystem I (PSI). Thus, the photosynthetic apparatus is one of the most iron-rich cellular systems. The PSI complexes of the model cyanobacterium *Synechocystis* sp. PCC 6803 (hereafter *Synechocystis* 6803) were estimated to contain 1.2 x 10^6 iron atoms per cell, about one order of magnitude more iron than an average *E. coli* cell [1,2]. Consequently, photosynthesis is fundamentally vulnerable to iron starvation, a situation that occurs frequently in nature [3]. However, the control of iron starvation responses is only partially understood in plants and phototrophic microorganisms.

Physiologically, the photosynthetic apparatus becomes strongly remodeled upon iron limitation [4–6][6]. The amounts of phycocyanin and chlorophyll become lowered [7,8], and photosynthetic intersystem electron transport is restricted [5]. Iron-containing proteins are substituted or reduced, including cytochrome b-559 of PSII (*psbEF* gene products), cytochromes b and f of the cytochrome b_6f complex and all the Fe/S cluster proteins, especially those of PSI [8–10].

Upon iron starvation, cyanobacteria reduce the relative number of PSI complexes, from a 4:1 PSI:PSII ratio to a 1:1 ratio (for overview, see [6]) and induce the chlorophyll-binding iron stress induced protein A [11,12]. The expression of proteins involved in iron transport and mobilization, such as FutABC, FeoB and ferritin, is induced [13]. Alternative redox carriers including copper-dependent plastocyanin (*petE* gene) and flavodoxin (*isiB* gene product) replace their iron-dependent counterparts cytochrome c553 or c6 (*petJ* gene) and ferredoxin 1 (Fed1) [9,14].

Studies of iron homeostasis in non-photosynthetic bacteria often revealed two key players involved in its regulation: the ferric uptake regulator (Fur), a transcription factor commonly considered a transcriptional repressor when bound to Fe^{2+}, and a small

regulatory RNA (sRNA), in enterobacteria called RyhB, which is controlled by Fur [15]. At higher iron concentrations, Fur binds Fe^{2+} to its regulatory site, leading to its dimerization, activation and DNA binding at specific DNA sequences, the Fur boxes in the promoter regions of relevant genes [16]. At lower iron concentrations, Fur loses the bound Fe^{2+}, becomes inactive, detaches from the DNA, and in *Synechocystis* 6803 it is eventually degraded by FtsH3 protease [17], and transcription of its target genes is derepressed. However, in cyanobacteria there is no evidence that any of the characterized transcription factors including FurA [18] would directly impact the expression of genes in the photosynthetic electron transport chain.

Therefore, we focused on sRNAs that would become specifically induced in this condition as potential functional analogs of RyhB. In *Synechocystis* 6803, an sRNA initially called NC-181 or Ncl1600 becomes highly induced upon iron deficiency [19,20]. We renamed this 68 nt sRNA as Iron Stress-Activated RNA1 (IsaR1). Here we comprehensively characterize the function of IsaR1 and demonstrate that IsaR1 has an essential regulatory role in the acclimation of the photosynthetic apparatus to iron starvation.

RESULTS

The sRNA IsaR1 is Widely Distributed in the Cyanobacterial Phylum

The sRNA IsaR1 in *Synechocystis* 6803 originates from the intergenic spacer between the *sll0033* gene encoding carotene isomerase CrtH and *sll0031* encoding the circadian clock-related light-dependent period modulator protein A (LdpA).

IsaR1 is widely conserved, including N_2 fixing and filamentous species, freshwater, marine, symbiotic, mesophilic and thermophilic cyanobacteria (**Figure S1**). In most genomes, *isaR1* is associated with the genes encoding uracil phosphoribosyltransferase (*upp)* or carotene isomerase *(crtH)*, or both (**Figure S1A**). IsaR1 sequences are characterized by a highly conserved region within the 5' segment and a sequence resembling a Rho-independent terminator of transcription (**Figure S1B**). This wide conservation of sequence, structure and synteny suggests a conserved function for IsaR1 in cyanobacteria.

Expression of IsaR1 is Specifically Enhanced by Iron Starvation and is under the Transcriptional Control of the Ferric Uptake Regulator

Northern blot experiments verified the strong expression of IsaR1 during iron starvation but weak or negligible expression under the other conditions tested (**Figure S1C**). Promoter fusion experiments revealed that IsaR1 expression is induced by iron starvation and that the dynamics resembled the activation of the *isiA* promoter (**Figure S2A**). The alignment of the *isaR1* upstream sequences from 31 cyanobacteria (**Figure S2B**) indicated the presence of a conserved sequence element resembling the Fur binding site for *isiA* [21]. In addition, the demonstration of the specific binding of recombinant FurA to the IsaR1 promoter (P_{isaR1}) and its loss upon the replacement of likely critical residues in the conserved sequence, supported the importance of this site for FurA-mediated regulation (**Figure S2C**).

Phenotypical Characterization of the IsaR1 Deletion and Complementation Mutants

A knockout mutant Δ*isaR1* in which *isaR1* was replaced by a kanamycin resistance gene and an inducible complementation strain, IsaR1comp, were subjected to iron starvation for 8 days by adding the iron chelator desferrioxamine B (DFB), while the P_{petE}–driven expression of IsaR1 in the complementation strain was induced by the addition of copper. Room temperature absorption spectra showed a stronger depigmentation in Δ*isaR1* than in the control (WT_pVZ) and the complemented strain IsaR1comp (**Figure 1A,B,C**). The complemented strain was phenotypically more like WT than Δ*isaR1*, the slight spectral differences between WT and IsaR1comp likely resulted from using the weaker ectopic P_{petE} promoter.

To identify possible effects on the photosynthetic apparatus, the impact of ectopic IsaR1 expression under non-stress conditions was studied in a time course experiment. For this purpose the vector with an extrachromosomal *isaR1* copy was introduced into *Synechocystis* 6803 WT yielding the overexpressing strain IsaR1OE. Addition of Cu^{2+} induced expression of IsaR1 from the copper-responsive P_{petE} promoter, while the iron concentration remained unchanged. Measuring the 77K fluorescence emission spectra of IsaR1OE and the WT_pVZ control before and after 2, 4, 8 and 11 days of induction revealed an increase in the ratio between the 685 nm and 726 nm peaks (corresponding to the PSII/PSI ratio) over time in IsaR1OE (**Figure 1D**). This result resembles the increase in the PSII/PSI ratio due to a decline in PSI numbers under iron depletion [4,22]. Only a slight decrease in the maximum quantum yield of PSII (defined as Fv/Fm) was observed in IsaR1OE (~25%) compared with WT_pVZ after 4 days of induction (**Figure 1F**). The Pm value, representing the maximum amount of photooxidizable P700, the primary donor of PSI, was less than

half in IsaR1OE (**Figure 1E**). Moreover, the performance of PSI under actinic light, measured as the effective photochemical yield of PSI, was remarkably lower in IsaR1OE than in the control (**Figure 1G**). Importantly, the decrease in PSI yield was accompanied by a higher acceptor side limitation of PSI in IsaR1OE (**Figure 1H**).

Characterization of the Transcriptomic Response to Iron Depletion in the IsaR1 Deletion Mutant Reveals a Highly Altered Iron Stress Response

We compared Δ*isaR1* transcriptomes in a time course experiment after the induction of iron starvation to the published *Synechocystis* 6803 WT response ([20] and **Data S1** and **S2)**. Despite its weak expression under iron-sufficient conditions (**Figure S1C**), the deletion of *isaR1* had a broad impact on the transcriptome (**Figure 2A**). The differentially abundant transcripts are presented in **Table S1** according to operons and encoded functions and include transcripts related to the uptake of inorganic carbon (C_i), the C_i-limitation responsive *flv4-flv2 (sll0217-sll0219*) flavodiiron protein operon, the NADPH dehydrogenase complex, motility, nitrogen assimilation and metabolism (**Figure 2A**). These results indicate a shift in the C-N metabolism in Δ*isaR1* and suggest a possible regulative role of IsaR1 under iron-replete conditions.

Whereas the levels of transcripts related to C_i, nitrogen assimilation and NADPH dehydrogenase converged during prolonged iron starvation in both strains, notable differences in the transcriptional response to iron stress appeared, as illustrated by the 48 h time point (**Figure 2B**). In agreement with the pronounced decreases in chlorophyll- and phycobilisome-dependent absorption in Δ*isaR1* at 48 h of iron depletion (**Figure 1**), the transcript levels of photosynthesis-related genes encoding allophycocyanin and phycocyanin, PSI and PSII components, and proteins involved in carbon fixation declined. In contrast, mRNAs for RNase E and RNase J, transposases,

psbZ, *rpoE*, several iron-containing proteins (*sodB*, *acnB*, *ssl0020/petF*, *sll1348*) and the Fe/S cluster biogenesis operon (*sufBCDS*) had stronger expression in the knockout. The genes with the strongest positive changes in Δ*isaR1* belonged to the *ssr3570-3572kpsMT* operon, which is possibly involved in extracellular lipopolysaccharide formation [23].

Computational Target Prediction and Analysis of Pulsed Overexpression Suggest Primary Targets of IsaR1

To elucidate the mode of action of IsaR1, we applied CopraRNA [24] using 20 IsaR1 homologs from various cyanobacteria to computationally predict IsaR1 targets. Functional enrichment analysis revealed a set of 38 candidate genes possibly controlled by IsaR1, belonging to the terms “iron ion containing”, “electron transport”, “metal ion binding, “photosynthesis”, “iron-sulfur cluster binding” and proteins with GAF-domains (**Figure 3A**). To enable the detection of *Synechocystis* 6803-specific targets that might have been missed by CopraRNA, we compared also the respective IntaRNA prediction [24] with the microarray results (**Data S2**).

We compared the transcriptome composition in IsaR1OE with an empty-vector control strain (WT_pVZ) at 6 h after *isaR1* induction, when it was ~25-fold overexpressed **(Figure S3)**. Potential targets are shown in **Figure 4**. The complete array results are summarized in **Data S2** and visualized in **Data S3**.

Excluding IsaR1, 41 transcripts had lower and 19 had higher expression in IsaR1OE. The upregulation of several C_i uptake-specific transcripts and of the mRNAs for glutamine synthetase inactivating factors *gifA* and *gifB* indicates a possible pleiotropic physiological response or shift in the C:N balance. Several mRNAs and 5’ UTRs among the 41 lower-expression target candidates were linked to photosynthesis and iron-containing proteins. In addition to the PSI-associated Fed1 (*petF, ssl0020*),

193 mRNAs affected by IsaR1 overexpression included the cytochrome b_6f complex (*petD,*
194 *petB, petA*), the iron-containing superoxide dismutase (*sodB*), the enzyme that
195 performs the first specific step of tetrapyrrole biosynthesis (*hemA*), cyanoglobin
196 (*slr2097*), the SufC subunit of the Suf Fe/S-cluster biogenesis complex (*ycf16*) and
197 some unknown or hypothetical proteins. The response regulators encoded by *sll1291*
198 (TaxP2), *slr1594* and *slr1214* (LsiR), and the CU-pili associated *slr1667* gene all were
199 expressed at a lower level in IsaR1OE. An inverse relationship was identified between
200 the higher accumulation of the 5' UTR of *slr0074* encoding SufB of the Fe/S cluster
201 biosynthesis complex and the mRNA, which was slightly decreased (**Figure 4**).
202 After the integration of the previous data, we investigated the following groups
203 in molecular detail: (i) the mobile electron carrier gene *petF1*; (ii) the iron-sulfur cluster
204 biogenesis genes, *sufBCDS*; (iii) the genes of the four major subunits of the
205 cytochrome b_6f complex, *petC1*, *petA, petB* and *petD*; (iv) genes involved in chlorophyll
206 and tetrapyrrole biosynthesis, *hemA, chlH, chlN*; and (v) genes for non-essential iron
207 containing proteins such as *sodB, acnB* and *ilvD*.
208
209 **Selected Reaction Monitoring (SRM) for Studying IsaR1 Target Proteins**
210 Changes at RNA level are not necessarily leading to changed protein
211 abundances. To study the effects of IsaR1 deletion and overexpression on the protein
212 profiles of the iron-depleted and iron-repleted cells, quantitative SRM-based
213 proteomics tailored to *Synechocystis* 6803 [10] was applied. SRM enables the precise
214 quantification also of low-abundance proteins and of membrane proteins. We
215 quantified the four proteins encoded by the *suf*-operon (SufBCDS), their transcriptional
216 regulator SufR [25], several other possible IsaR1 targets and a set of control proteins.
217 Altogether, the expression levels of 42 proteins in IsaR1OE and WT_pVZ, as well as
218 in Δ*isaR1* (**Tables S5 and S6**) and the WT control were investigated using SRM in two

219 independent time course experiments (0, 24 and 96 h after inducing IsaR1
220 overexpression or at 0, 5, 24, 48 and 96 h after the removal of iron). To allow time for
221 translation, an offset for the proteomics was chosen in comparison with the
222 transcriptomic analysis. The respective log_2-fold changes of the detected protein levels
223 in IsaR1OE compared with WT_pVZ are represented in **Figure 3B** and the specific
224 results described below, in context with the other data.
225
226 **PSI-Associated Ferredoxin I is a Major Target of IsaR1**
227 The mRNA encoding Fed1 (*petF*) was predicted as the number 1 IsaR1 target by
228 CopraRNA (**Data S2** and **Figure 3A**). Consistent with this prediction, the typical strong
229 downregulation of *petF* transcript accumulation under iron deprivation was missing in
230 Δ*isaR1* (**Figure 5A**). Furthermore, the ectopic overexpression of IsaR1 under iron-
231 replete conditions led to the rapid disappearance of *petF* mRNA (**Figure 4**) and a
232 corresponding reduction of the Fed1 protein, to less than 30% of the initial value at 96
233 h after the induction of IsaR1, whereas the WT control did not show a reduction(**Figure**
234 **5B**).
235 The IntaRNA prediction suggested an extended interaction between IsaR1 and
236 the *petF* 5' UTR, including the ribosome binding site (**Figure 5D**). To corroborate the
237 *petF* mRNA as a direct IsaR1 target, we used the heterologous superfolder GFP
238 (sGFP) reporter system established for the verification of sRNA targets in
239 enterobacteria [26] and cyanobacteria [27]. The co-expression of IsaR1 with the *petF*
240 5' UTR fused to *sgfp* in *E. coli* resulted in a significant 4.8 ± 0.8-fold repression of
241 fluorescence (**Figure 5C**). Hence, the *petF* mRNA encoding Fed1, appears as a direct
242 target of IsaR1.
243
244 **The Cytochrome b_6f Complex as a Target of IsaR1**

The expression of genes encoding subunits of the cytochrome b_6f complex decreased during iron starvation in WT but less so in Δ*isaR1* (**Figure 5G**). Out of these, *petA*, *petB* and *petD* were identified by CopraRNA or IntaRNA as putative IsaR1 targets (**Figure 3A; Data S2**). IsaR1 overexpression negatively affected the *petC1A* and *petBD* transcript accumulation under non-stress conditions (**Figure 5E**) and led to a corresponding reduction of cytochrome f and PetC1 at the protein level, whereas the WT control did not show any reduction (**Figure 5E,F**). These results strongly suggest that the previously observed reduction in cytochrome b_6f complex accumulation during prolonged iron starvation (**Figure 5G** and references [4,5,28]) is largely mediated by IsaR1, targeting multiple different mRNAs.

Iron-Sulfur Biogenesis is a Major Target of IsaR1

The *sufBCDS* operon encodes essential components for the biosynthesis of Fe/S clusters and appears vital for survival as the genes cannot be deleted [29]. Two TSSs were mapped for *sufB/ycf24,* 267 (TSS1) and 119 nt (TSS2) upstream of the start codon (**Figure 6A**). TSS2 was the tenth-most strongly induced TSS during iron deprivation [19], but the mRNA steady-state level was only slightly induced (**Figure 6E**). Moreover, our results show a repressive effect of IsaR1 on the *sufBCDS* transcript accumulation at 6 h of ectopic overexpression of IsaR1 (**Figure 6A**) and the appearance of an sRNA, SufZ, that originated from TSS2 in an iron stress-dependent manner, strictly correlating with the presence of IsaR1, as it remained undetectable in Δ*isaR1* at all times and appeared earlier in IsaR1OE (**Figure 6B**).

Consistently, the levels of the mRNA section of the *suf* operon and the Suf proteins remained constant at iron depletion in the WT, whereas they were strongly induced in Δ*isaR1*. SufR, the transcriptional repressor of the *sufBCDS* operon showed an inverse response in WT and Δ*isaR1* (**Figure 6E**). In addition, all four proteins from

the *sufBCDS* operon were strongly downregulated in IsaR1OE at 96 h compared with the control (log_2FC: SufB, -1.34-fold; SufC, -1.15-fold; SufD, -0.79-fold; SufS, -1.07-fold, **Figure 3B**). Interestingly, SufR, with a log_2 factor of 1.05, was the most up-regulated protein in IsaR1OE after 96 h of induction, further illustrating the complex regulation of this operon. The first gene of the *suf* operon, *sufB*, was ranked 2 in the CopraRNA prediction (**Figure 3A** and **Data S2**). When its 5' UTR was fused to *sgfp,* the co-expression of IsaR1 in *E. coli* resulted in a 4.6±1.8-fold repression of the fluorescence signal. A change of two nucleotides (GU to UA) within the predicted interaction site diminished the IsaR1-mediated repression of *sgfp* fluorescence to 2.4±0.8-fold, and compensatory mutations in the 5' UTR re-established the full 6.2±3.7-fold repression (**Figure 6C** and **Figure S4**). Thus, *sufB* was unambiguously confirmed as an IsaR1 target. We conclude that IsaR1 caps *sufBCDS* expression under iron starvation and generates SufZ as a by-product.

The Expression of Genes Encoding Several Iron-Containing Proteins and Chlorophyll and Tetrapyrrole Biosynthesis Enzymes is Affected by IsaR1

The tetrapyrrole and chlorophyll biosynthesis enzymes encoded by *hemA* (rank 9 CopraRNA)*, chlN* (rank 32 CopraRNA) and *chlH* (rank 61 IntaRNA) were potential targets of IsaR1 (**Figure 3A**). Both *hemA* and *chlH* responded in the IsaR1OE microarrays (**Figure 4**). To further verify a direct repression, we conducted an sGFP assay in *E. coli* for *hemA* and *chlN* and observed more than 2-fold repression of GFP fluorescence upon IsaR1 co-expression (**Figure S4**).

Several additional IsaR1 targets were suggested by prediction, transcriptomics and proteomics (summarized in **Figure 7**). The mRNAs for the iron-containing form of superoxide dismutase (*sodB*), aconitate hydratase (*acnB*) and dihydroxy-acid dehydratase (*ilvD*) ranked highly in the predictions (**Figure 3A**), and transcript levels

297 declined with ectopic IsaR1 expression (**Figure 4**). Both *sodB* and *acnB* mRNAs
298 accumulated at an elevated level in Δ*isaR1* during iron stress (**Figure 2B**), similar to
299 *petF* and the *suf* operon transcripts. Moreover, all these 5' UTRs were controlled by
300 IsaR1 in the sGFP assay (**Figure S5**) and SodB and AcnB proteins were repressed by
301 IsaR1OE in the SRM assay; SodB by 1.27-fold, and AcnB by 1.19-fold (log_2-fold
302 changes; **Figure 3B**).
303
304 **DISCUSSION**
305 **Disentanglement of Iron Starvation Regulation**
306 Although the physiological responses of photosynthetic organisms to iron limitation
307 have been well studied, the knowledge of the regulatory factors behind these dynamic
308 acclimation responses has remained scarce. The transcriptional repressor FurA
309 cannot convey iron starvation-dependent repression because it requires Fe^{2+} for DNA
310 binding. We show that the sRNA IsaR1 fulfills this repressor function in iron
311 homeostasis. It regulates the expression of several genes relevant to photosynthetic
312 electron transfer, pigment biosynthesis, Fe/S cluster biogenesis, as well as additional
313 iron cofactor-containing proteins, e.g., [Fe-Ni] hydrogenase subunits, and potentially
314 even regulators involved in phototaxis. Targets that can be unambiguously assigned
315 to IsaR1 include Fed1, cytochrome c6 (PetJ), the iron sulfur biogenesis proteins
316 SufBCDS, the superoxide dismutase subunit SodB, the cytochrome b_6f complex
317 proteins PetABDC1, aconitate hydratase (AcnB) and the tetrapyrrole biosynthesis
318 enzymes HemA and ChlN. Interestingly, *acnB* and *sodB* are also targets of RyhB in *E.*
319 *coli* [30]. IsaR1 functions through a single seed region (**Figure S7**) that may also be
320 used by its homologs in other cyanobacteria. An overview of the proposed IsaR1
321 regulon and its connections to the Fur and SufR regulons is presented in **Figure 7** and
322 **Table S3**.

IsaR1 and Ferredoxin

A main target of IsaR1 is Fed1, which is the major acceptor of electrons from PSI. Overexpression of IsaR1 led to decreased Fed1 amounts (**Figure 5B**), which can explain the observed acceptor side limitation of PSI in IsaR1OE (**Figure 1E**). This is highly relevant as Fed1 is the most abundant ferredoxin, mediating several major redox processes, including the electron transfer from PSI [31] to ferredoxin NADP reductase that reduces $NADP^+$ for CO_2 fixation, nitrogen assimilation, sulfite reduction, fatty acid metabolism and others ([32]). Our results provide a mechanistic explanation for the observation that *petF* expression in cyanobacteria during iron starvation is regulated at the level of mRNA stability [33]. In addition, the SRM analysis revealed an impact of IsaR1 overexpression on other ferredoxins, Fed4 (*slr0150*, -0.79 log_2-fold) and Fed5 (*slr0148*, -0.95 log_2-fold). Both bind Fe/S clusters as cofactors and might be indirectly affected by the repression of their biogenesis. Notably, two more Fed and Fed-like genes (*ssr3184* / *fed8* and *slr1205*) appeared in the CopraRNA prediction.

Regulation of the Suf Operon

The SUF complex is the essential Fe/S cluster assembly system in *Synechocystis* 6803 [29]. Our data consistently showed *sufB* and the *suf* operon as direct targets of IsaR1. This regulation is physiologically relevant because *suf* mRNA and protein levels were strongly correlated in all strains and conditions investigated (**Figure 6C**). The regulation of the capacity to produce Fe/S clusters under iron stress appears to take place mainly via the *suf* operon because other genes involved in Fe/S biogenesis such as *sufA, iscA, nfuA, iscS1, iscS2, iscR* and *rubA* [29] show only minor changes in response to iron depletion [20]. A regulator of the *suf* operon is the transcriptional repressor SufR, which is also an auto-repressor [25,34,35].

DNA binding by SufR depends on the presence and redox state of complexed Fe/S clusters (holo-SufR). When the capacity to provide Fe/S clusters is low, SufR appears more in the apo-form. While holo-SufR binds strongly to the *suf* promoter and represses the *suf*-operon under iron sufficient conditions, the apo-form has a low affinity to the *suf* promoter, and *suf* operon transcription can proceed [34]. This is efficient to regulate Fe/S cluster biogenesis in iron sufficient conditions via a feedback loop. However, when the Fe/S biogenesis capacity is limited by iron availability this end-product repression-type regulation would lead to a constitutive transcriptional induction of the *suf* operon, which is not physiological.

Therefore, another repressor is necessary under iron starvation conditions to control Suf protein expression. We show that IsaR1 performs this function, and thus resembles the role of RyhB, which under iron deprivation controls the expression of Fe-S cluster assembly proteins in *E. coli*, such as *iscRSUA* operon and *erpA* [30,36,37]. In summary, the *suf* operon is transcriptionally de-repressed during iron starvation, but this activation is counteracted by the post-transcriptional repressor IsaR1.This is in agreement with the observed repression of Suf transcripts and proteins in the SufR inactivation strain under iron depletion [35].

IsaR1 Acts on the Photosynthetic Apparatus in Three Ways

IsaR1 directly interferes with the expression of several genes encoding proteins for the photosynthetic electron transport chain. This includes the four major cytochrome b_6f proteins and the mobile electron carrier cytochrome c6 that transfers electrons from cytochrome b_6f to PSI and Fed1, the major electron acceptor from PSI. There is also evidence that PSI and PSII proteins such as PsbE and PsaA/B might be directly controlled by IsaR1 (**Figure S4** and **S6)**. In addition, the effects of IsaR1 on the *suf* operon and on *hemA* affect the photosynthetic apparatus indirectly. The *suf* operon

encodes an essential enzymatic system for the synthesis of Fe/S clusters in *Synechocystis* 6803, whereas *hemA* encodes glutamyl-tRNA reductase, producing the first committed intermediate of the C5 pathway. This pathway is the only means for producing tetrapyrroles, chlorophylls, heme groups and several chromophores in this organism. Chlorophyll biosynthesis is further affected by the regulation of *chlN* and *chlH*.

The availability of chlorophyll and Fe/S clusters is crucial for the assembly and stability of photosystems I/II and cytochrome b_6f complexes [38,39]. Therefore, IsaR1 impacts the photosynthetic apparatus in three fundamentally different ways: (i) by regulating certain mRNAs directly; (ii) via the Fe/S cluster biosynthetic pathway; (iii) via the tetrapyrrole biosynthesis chain. The fact that a 68 nt-long riboregulator controls a network of this complexity **(Figure 7)** is impressive.

Author Contributions

WRH and JG planned the project. GK, VS, TH and MM generated and characterized the mutant strains. JG performed the bioinformatics analyses, and JG, GK, LV, TH, SK, YA, MEF, EMA and WRH analyzed data. DB and SK performed *luxAB* reporter gene assays, TK and YH EMSA, and JG, GK and LV prepared the figures. All authors contributed to the manuscript. The authors declare no conflicts of interests.

ACKNOWLEDGMENTS

This work was supported by a German Federal Ministry of Education and Research grant “e:bio RNAsys” 0316165, DFG grant HE 2544/9-1 (to WRH), Academy of Finland grants #253269, #271832 and #273870 (to EMA), Portuguese Fundação para a Ciência e a Tecnologia grants IF/00881/2013 and UID/Multi/04326/2013–CCMAR (to MEF) and by the EU ITN “Photo.COMM” (to WRH, EMA and GK). We thank Gudrun Krüger and Viktoria Reimann for support in the microarray experiments and the Biocenter Finland and the Proteomics Facility of the Turku Centre for Biotechnology for support in the SRM experiments. We thank Miguel Hernández-Prieto for suggestions about Fur boxes, Christian Weingärtner for help with mutant analysis, Andreas Richter for the first target predictions, and Heiko Lokstein and Claudia Steglich for the introduction to spectroscopic analysis.

REFERENCES

1. Finney, L.A., and O'Halloran, T.V. (2003). Transition metal speciation in the cell: insights from the chemistry of metal ion receptors. Science *300*, 931–936.

2. Keren, N., Aurora, R., and Pakrasi, H.B. (2004). Critical roles of bacterioferritins in iron storage and proliferation of cyanobacteria. Plant Physiol. *135*, 1666–1673.

3. Behrenfeld, M., and Kolber, Z.S. (1999). Widespread iron limitation of phytoplankton in the South Pacific Ocean. Science *283*, 840–843.

4. Fraser, J.M., Tulk, S.E., Jeans, J.A., Campbell, D.A., Bibby, T.S., and Cockshutt, A.M. (2013). Photophysiological and photosynthetic complex changes during iron starvation in *Synechocystis* sp. PCC 6803 and *Synechococcus elongatus* PCC 7942. PloS One *8*, e59861.

5. Ivanov, A.G., Park, Y.I., Miskiewicz, E., Raven, J.A., Huner, N.P., and Oquist, G. (2000). Iron stress restricts photosynthetic intersystem electron transport in *Synechococcus* sp. PCC 7942. FEBS Lett. *485*, 173–177.

6. Straus, N.A. (2004). Iron Deprivation: Physiology and Gene Regulation. In The Molecular Biology of Cyanobacteria (Dordrecht, The Netherlands: Kluwer Academic Publisher), pp. 731–750.

7. Guikema, J.A., and Sherman, L.A. (1983). Organization and function of chlorophyll in membranes of cyanobacteria during iron starvation. Plant Physiol. *73*, 250–256.

8. Sandmann, G. (1985). Consequences of iron deficiency on photosynthetic and respiratory electron transport in blue-green algae. Photosynth. Res. *6*, 261–271.

9. Sandmann, G., and Malkin, R. (1983). Iron-sulfur centers and activities of the photosynthetic electron transport chain in iron-deficient cultures of the blue-green alga *Aphanocapsa*. Plant Physiol. *73*, 724–728.

10. Vuorijoki, L., Isojärvi, J., Kallio, P., Kouvonen, P., Aro, E.-M., Corthals, G.L., Jones, P.R., and Muth-Pawlak, D. (2016). Development of a quantitative SRM-based proteomics method to study iron metabolism of *Synechocystis* sp. PCC 6803. J. Proteome Res. *15*, 266–279.

11. Burnap, R.L., Troyan, T., and Sherman, L.A. (1993). The highly abundant chlorophyll-protein complex of iron-deficient *Synechococcus* sp. PCC7942 (CP43') is encoded by the isiA gene. Plant Physiol. *103*, 893–902.

12. Laudenbach, D.E., and Straus, N.A. (1988). Characterization of a cyanobacterial iron stress-induced gene similar to psbC. J. Bacteriol. *170*, 5018–5026.

13. Shcolnick, S., Summerfield, T.C., Reytman, L., Sherman, L.A., and Keren, N. (2009). The mechanism of iron homeostasis in the unicellular cyanobacterium *Synechocystis* sp. PCC 6803 and its relationship to oxidative stress. Plant Physiol. *150*, 2045–2056.

14. Hutber, G.N., Hutson, K.G., and Rogers, L.J. (1977). Effect of iron deficiency on levels of two ferredoxins and flavodoxin in a cyanobacterium. FEMS Microbiol. Lett. *1*, 193–196.

15. Massé, E., and Gottesman, S. (2002). A small RNA regulates the expression of genes involved in iron metabolism in *Escherichia coli*. Proc. Natl. Acad. Sci. U. S. A. *99*, 4620–4625.

16. Pecqueur, L., D'Autréaux, B., Dupuy, J., Nicolet, Y., Jacquamet, L., Brutscher, B., Michaud-Soret, I., and Bersch, B. (2006). Structural changes of *Escherichia coli* ferric uptake regulator during metal-dependent dimerization and activation explored by NMR and X-ray crystallography. J. Biol. Chem. *281*, 21286–21295.

17. Krynická, V., Tichý, M., Krafl, J., Yu, J., Kaňa, R., Boehm, M., Nixon, P.J., and Komenda, J. (2014). Two essential FtsH proteases control the level of the Fur repressor during iron deficiency in the cyanobacterium *Synechocystis* sp. PCC 6803. Mol. Microbiol. *94*, 609–624.

18. González, A., Angarica, V.E., Sancho, J., and Fillat, M.F. (2014). The FurA regulon in *Anabaena* sp. PCC 7120: in silico prediction and experimental validation of novel target genes. Nucleic Acids Res. *42*, 4833–4846.

19. Kopf, M., Klähn, S., Scholz, I., Matthiessen, J.K.F., Hess, W.R., and Voß, B. (2014). Comparative analysis of the primary transcriptome of *Synechocystis* sp. PCC 6803. DNA Res. *21*, 527–539.

20. Hernández-Prieto, M.A., Schön, V., Georg, J., Barreira, L., Varela, J., Hess, W.R., and Futschik, M.E. (2012). Iron deprivation in *Synechocystis*: inference of pathways, non-coding RNAs, and regulatory elements from comprehensive expression profiling. G3 Bethesda Md *2*, 1475–1495.

21. Kunert, A., Vinnemeier, J., Erdmann, N., and Hagemann, M. (2003). Repression by Fur is not the main mechanism controlling the iron-inducible isiAB operon in the cyanobacterium *Synechocystis* sp. PCC 6803. FEMS Microbiol. Lett. *227*, 255–262.

22. Schrader, P.S., Milligan, A.J., and Behrenfeld, M.J. (2011). Surplus photosynthetic antennae complexes underlie diagnostics of iron limitation in a cyanobacterium. PloS One *6*, e18753.

23. Nsahlai, C.J., and Silver, R.P. (2003). Purification and characterization of KpsT, the ATP-binding component of the ABC-capsule exporter of *Escherichia coli* K1. FEMS Microbiol. Lett. *224*, 113–118.

24. Wright, P.R., Georg, J., Mann, M., Sorescu, D.A., Richter, A.S., Lott, S., Kleinkauf, R., Hess, W.R., and Backofen, R. (2014). CopraRNA and IntaRNA: predicting small RNA targets, networks and interaction domains. Nucleic Acids Res. *42*, W119-123.

25. Wang, T., Shen, G., Balasubramanian, R., McIntosh, L., Bryant, D.A., and Golbeck, J.H. (2004). The sufR gene (sll0088 in *Synechocystis* sp. strain PCC 6803) functions as a repressor of the sufBCDS operon in iron-sulfur cluster biogenesis in cyanobacteria. J. Bacteriol. *186*, 956–967.

26. Corcoran, C.P., Podkaminski, D., Papenfort, K., Urban, J.H., Hinton, J.C.D., and Vogel, J. (2012). Superfolder GFP reporters validate diverse new mRNA targets of the classic porin regulator, MicF RNA. Mol. Microbiol. *84*, 428–445.

27. Georg, J., Dienst, D., Schürgers, N., Wallner, T., Kopp, D., Stazic, D., Kuchmina, E., Klähn, S., Lokstein, H., Hess, W.R., *et al.* (2014). The small regulatory RNA SyR1/PsrR1 controls photosynthetic functions in cyanobacteria. Plant Cell *26*, 3661–3679.

28. Sandström, S., Ivanov, A.G., Park, Y.-I., Oquist, G., and Gustafsson, P. (2002). Iron stress responses in the cyanobacterium *Synechococcus* sp. PCC7942. Physiol. Plant. *116*, 255–263.

496 29. Balasubramanian, R., Shen, G., Bryant, D.A., and Golbeck, J.H. (2006). Regulatory
497 roles for IscA and SufA in iron homeostasis and redox stress responses in the
498 cyanobacterium *Synechococcus* sp. strain PCC 7002. J. Bacteriol. *188*, 3182–
499 3191.

500 30. Massé, E., Vanderpool, C.K., and Gottesman, S. (2005). Effect of RyhB small RNA
501 on global iron use in *Escherichia coli*. J. Bacteriol. *187*, 6962–6971.

502 31. Lelong, C., Boekema, E.J., Kruip, J., Bottin, H., Rögner, M., and Sétif, P. (1996).
503 Characterization of a redox active cross-linked complex between cyanobacterial
504 photosystem I and soluble ferredoxin. EMBO J. *15*, 2160–2168.

505 32. Cassier-Chauvat, C., and Chauvat, F. (2014). Function and Regulation of
506 Ferredoxins in the Cyanobacterium, *Synechocystis* PCC6803: Recent Advances.
507 Life Basel Switz. *4*, 666–680.

508 33. Bovy, A., de Vrieze, G., Lugones, L., van Horssen, P., van den Berg, C., Borrias,
509 M., and Weisbeek, P. (1993). Iron-dependent stability of the ferredoxin I transcripts
510 from the cyanobacterial strains *Synechococcus* species PCC 7942 and *Anabaena*
511 species PCC 7937. Mol. Microbiol. *7*, 429–439.

512 34. Shen, G., Balasubramanian, R., Wang, T., Wu, Y., Hoffart, L.M., Krebs, C., Bryant,
513 D.A., and Golbeck, J.H. (2007). SufR coordinates two [4Fe-4S]2+, 1+ clusters and
514 functions as a transcriptional repressor of the sufBCDS operon and an
515 autoregulator of sufR in cyanobacteria. J. Biol. Chem. *282*, 31909–31919.

516 35. Vuorijoki, L., Tiwari, A., Kallio, P., and Aro, E.-M. (2017). Inactivation of iron-sulfur
517 cluster biogenesis regulator SufR in Synechocystis sp. PCC 6803 induces unique
518 iron-dependent protein-level responses. Biochim. Biophys. Acta *1861*, 1085–1098.

519 36. Desnoyers, G., Morissette, A., Prévost, K., and Massé, E. (2009). Small RNA-
520 induced differential degradation of the polycistronic mRNA iscRSUA. EMBO J. *28*,
521 1551–1561.

522 37. Mandin, P., Chareyre, S., and Barras, F. (2016). A Regulatory Circuit Composed
523 of a Transcription Factor, IscR, and a Regulatory RNA, RyhB, Controls Fe-S
524 Cluster Delivery. mBio *7*. Available at:
525 http://www.ncbi.nlm.nih.gov/pmc/articles/PMC5040110/ [Accessed March 17,
526 2017].

527 38. Kopečná, J., Sobotka, R., and Komenda, J. (2013). Inhibition of chlorophyll
528 biosynthesis at the protochlorophyllide reduction step results in the parallel
529 depletion of Photosystem I and Photosystem II in the cyanobacterium
530 *Synechocystis* PCC 6803. Planta *237*, 497–508.

531 39. Touraine, B., Boutin, J.-P., Marion-Poll, A., Briat, J.-F., Peltier, G., and Lobréaux,
532 S. (2004). Nfu2: a scaffold protein required for [4Fe-4S] and ferredoxin iron-sulphur
533 cluster assembly in Arabidopsis chloroplasts. Plant J. Cell Mol. Biol. *40*, 101–111.

534 40. Trautmann, D., Voss, B., Wilde, A., Al-Babili, S., and Hess, W.R. (2012).
535 Microevolution in cyanobacteria: re-sequencing a motile substrain of
536 *Synechocystis* sp. PCC 6803. DNA Res. *19*, 435–448.

537 41. Rippka, R., Deruelles, J., Waterbury, J.B., Herdman, M., and Stanier, R.Y. (1979).
538 Generic assignments, strain histories and properties of pure cultures of
539 cyanobacteria. J. Gen. Microbiol. *111*, 1–61.

42. Shcolnick, S., Shaked, Y., and Keren, N. (2007). A role for mrgA, a DPS family protein, in the internal transport of Fe in the cyanobacterium *Synechocystis* sp. PCC6803. Biochim. Biophys. Acta *1767*, 814–819.

43. Mitschke, J., Georg, J., Scholz, I., Sharma, C.M., Dienst, D., Bantscheff, J., Voß, B., Steglich, C., Wilde, A., Vogel, J., *et al.* (2011). An experimentally anchored map of transcriptional start sites in the model cyanobacterium *Synechocystis* sp. PCC6803. Proc. Natl. Acad. Sci. *108*, 2124–2129.

44. Klähn, S., Baumgartner, D., Pfreundt, U., Voigt, K., Schön, V., Steglich, C., and Hess, W.R. (2014). Alkane biosynthesis genes in cyanobacteria and their transcriptional organization. Front. Bioeng. Biotechnol. *2*, 24.

45. Hernández, J.A., López-Gomollón, S., Muro-Pastor, A., Valladares, A., Bes, M.T., Peleato, M.L., and Fillat, M.F. (2006). Interaction of FurA from Anabaena sp. PCC 7120 with DNA: a reducing environment and the presence of Mn2+ are positive effectors in the binding to isiB and furA promoters. Biometals *19*, 259–268.

46. Pinto, F.L., Thapper, A., Sontheim, W., and Lindblad, P. (2009). Analysis of current and alternative phenol based RNA extraction methodologies for cyanobacteria. BMC Mol. Biol. *10*, 79.

47. Ritchie, M.E., Phipson, B., Wu, D., Hu, Y., Law, C.W., Shi, W., and Smyth, G.K. (2015). limma powers differential expression analyses for RNA-sequencing and microarray studies. Nucleic Acids Res. *43*, e47.

48. MacLean, B., Tomazela, D.M., Shulman, N., Chambers, M., Finney, G.L., Frewen, B., Kern, R., Tabb, D.L., Liebler, D.C., and MacCoss, M.J. (2010). Skyline: an open

562 source document editor for creating and analyzing targeted proteomics
563 experiments. Bioinforma. Oxf. Engl. *26*, 966–968.

564 49. Choi, M., Chang, C.-Y., Clough, T., Broudy, D., Killeen, T., MacLean, B., and Vitek,
565 O. (2014). MSstats: an R package for statistical analysis of quantitative mass
566 spectrometry-based proteomic experiments. Bioinforma. Oxf. Engl. *30*, 2524–
567 2526.

568 50. Sharma, V., Eckels, J., Taylor, G.K., Shulman, N.J., Stergachis, A.B., Joyner, S.A.,
569 Yan, P., Whiteaker, J.R., Halusa, G.N., Schilling, B., *et al.* (2014). Panorama: A
570 targeted proteomics knowledge base. J. Proteome Res. *13*, 4205–4210.

571

572 **Figure Legends**

573

574 **Figure 1. Phenotypes of Δ*isaR1,* IsaR1 complementation and overexpression**
575 **strains compared with the control strain WT_pVZ (WT carrying empty plasmid**
576 **pVZ322::pPetE::oop). (A)** Room temperature absorption spectra of WT, Δ*isaR1* and
577 IsaR1comp cell cultures before (0 d, continuous lines) and after (8 d, broken lines) the
578 addition of 100 μM DFB (iron chelator) and 2 μM $CuSO_4$ (induction of the P_{petE} promoter
579 for the complementation of IsaR1). The results from three independent biological
580 replicates were averaged. The spectra were normalized to OD_{750} to help evaluate their
581 structure.
582 **(B)** WT, Δ*isaR1* and IsaR1comp cell cultures 8 d after induction.
583 **(C)** Decrease of chlorophyll and phycocyanin absorptions in WT, Δ*isaR1* and IsaR1
584 comp cell cultures during iron limitation. Phycocyanin peak absorption was measured
585 at 635 nm. Because of the blue shift of the chlorophyll peak during iron limitation, the
586 chlorophyll absorption maximum wavelength changed from 686 nm to 678 nm. (A.U.–
587 arbitrary units, Chl– chlorophyll, PC– phycocyanin).
588 **(D)** The 77K fluorescence spectra of IsaR1OE and WT_pVZ before induction (0 d) and
589 at 4 d after induction with 2 μM $CuSO_4$. The fluorescence spectra were measured at
590 440 nm excitation. The chlorophyll content of the samples was adjusted to 7.5 μg Chl
591 a/mL. The fluorescence spectra were normalized to 726 nm (PSI). Inset top right – 685
592 nm/726 nm peak ratio (indicating PSII:PSI ratio) in IsaR1OE and WT_pVZ control over
593 the course of induction.
594 **(E)** Maximum amount of oxidizable P700 (Pm) before and after 4d of IsaR1 induction
595 (two biological replicates). **(F)** The maximum quantum yield of PSII (Fv/Fm) in the
596 presence of 20 μM DCMU (two biological replicates). **(G)** Effective photochemical

quantum yield of PSI, Y(I). **(H)** Acceptor side limitation of PSI, Y(NA), in WT_pVZ and IsaR1OE before and after 96 h of IsaR1 induction. Mean ± SD, two biological replicates.

Figure 2. **Transcriptome differences between Δ*isaR1* and WT under standard conditions (A) and after 48 h of iron depletion by DFB addition (B).** Volcano plots: Log-transformed fold changes (FC) between Δ*isaR1* and WT (x-axis, difference of $\log_2$ expression values) and $-\log_{10}$ (adj. p-value) (y-axis). Broken lines indicate the adj. p-value threshold of 0.05 and FC thresholds of 1 and -1. Functional groups are color-coded. Functional characterization was performed for all genes in the Δ*isaR1* - WT comparison with a significant FC at one or more of the time points after DFB addition (0 h, 3 h, 12 h, 24 h, 48 h, or 72 h). The differentially abundant transcripts were sorted according to operons and encoded functions in **Table S1**. Details are shown in the genome-wide expression plot (**Data S1**) and numeric values presented in **Data S2**.

Figure 3. Prediction of IsaR1 targets. (A) CopraRNA target prediction for IsaR1. The 38 most promising predicted targets are shown, including the top 20 predictions and those in the top 100 list which were enriched in one of the 6 displayed functional groups. The complete prediction is presented in **Data S2.** The top-ranking target, *upp*, was excluded because its 5' UTR is located directly antisense to *isaR1* in many cyanobacteria, leading to an artificially good prediction p-value. This is different in *Synechocystis* 6803; hence, we excluded *upp* from our analysis. **(B)** Results of selected reaction monitoring proteomics of the IsaR1OE time course 0, 24 and 96 h after induction. Only proteins with an adj. p-value ≤0.05 at time point 96 h and absolute $\log_2$fold change <0.8 at time point 0 h are displayed. The differentially abundant proteins are given in **Table S2** according to operons and encoded functions.

623

624 **Figure 4. Transcriptome differences in IsaR1OE and the control after 6 h pulse**
625 **expression of IsaR1, when it was ~25-fold overexpressed (Figure S3).** X-axis:
626 copper response of IsaR1OE with IsaR1 overexpression versus the copper only
627 response of the control. Y-axis: transcript levels in IsaR1OE versus that of the control
628 strain at 6 h after copper addition. Transcripts that showed differences before copper
629 addition are not considered. Transcript names are shown in black for transcripts with
630 an absolute $\log_2$-fold change of ≥0.9 in either condition and in red or blue for
631 CopraRNA/IntaRNA top 100 predicted targets with an absolute fold change of ≥0.5 in
632 either condition. CopraRNA prediction overrules IntaRNA prediction. IsaR1 is not
633 shown in this plot. The complete set of transcriptome differences and predicted targets
634 is presented in **Data S2,** the genome-wide expression plot for the pulsed
635 overexpression of IsaR1 at iron replete conditions in **Data S3.**
636

637 **Figure 5. The major ferredoxin Fed1 and the cytochrome *b_6f* complex as IsaR1**
638 **targets. (A)** The *petF* gene (*ssl0020*) that encodes ferredoxin I. Time course of the
639 iron stress microarray experiment for WT and Δ*isaR1*. For each time point, the error
640 bars were calculated from two independent microarray experiments. The transcript
641 level began to decline 12 h after the onset of iron stress in WT and continued to decline
642 over 3 d. In contrast, the Δ*isaR1* mutant showed a much weaker and delayed reduction
643 of the expression level. For additional details, see the legend to **Data 1**.
644 **(B)** The Fed1 protein level decreased gradually in IsaR1OE, to approximately 50%
645 after 24 h and approximately 20% after 96 h of Cu^{2+}-induced IsaR1 overexpression. A
646 Western blot with an antiserum against the D1 protein is shown for comparison.
647 **(C)** Verification of the IsaR1–*petF* interaction in a heterologous reporter assay. Density
648 plot of the fluorescence of representative replicates (10000 events each) from the flow

cytometer experiment for cells carrying no GFP (background fluorescence, black), the *petF*-UTR translationally fused to sGFP in the presence of control plasmid pJV300 (red) or in the presence of IsaR1 (blue). Inset bottom left: Repression of the GFP fluorescence by IsaR1 as measured from 6 independent clones. The fold repression is the ratio of the GFP fluorescence of the respective translational 5′ UTR *sgfp* fusion in the presence of the control plasmid pJV300 and a plasmid for the expression of the respective IsaR1 variant, after the subtraction of the background fluorescence (details in **Figure S4** and **S5**).

(D) Predicted interaction between the *petF* 5' UTR and IsaR1 (for comparison to other interactions, see **Figure S7**). The putative ribosome binding site and start codon are boxed.

(E) Left: iron stress time course showing transcript levels of *petB, petD, petA,* and *petC1* detected via microarray in the WT_pVZ and IsaR1OE strains at 6 h after induction with Cu^{2+}. The error bars were calculated from two independent microarray experiments for each time point. Right: protein expression of PetC1 after 96 h Cu^{2+} induction in IsaR1OE and WT_pVZ strains based on SRM assays. The error bars were calculated from 3 independent SRM experiments.

(F) Protein expression of cytochrome F (*petA*) in a time course experiment in WT and IsaR1OE. One representative Western blot is shown. The error bars were calculated from three independent biological replicates.

(G) Transcript levels of four mRNAs encoding the four major cytochrome b_6f proteins during an iron depletion time course in WT and Δ*isaR1*. Data were taken from the iron stress microarray experiment, and the error bars were calculated from two independent experiments for each time point.

…

674 **Figure 6. The *sufBCDS* operon as a IsaR1 target. (A)** Visualization of the *sufR-sufB*
675 intergenic and promoter region. UTRs are shown as white boxes, and genes are shown
676 as black boxes. The read numbers for primary transcripts from a dRNAseq experiment
677 after 24 h of iron stress (grey) or exponential growth phase (white) were taken from
678 reference [19] and square-root transformed (right y-axis). From this mapping, TSS1
679 and TSS2 (bent arrows) were inferred upstream of the *sufBCDS* operon, at positions
680 2871408 and 2871555, respectively. The expression levels from the IsaR1
681 overexpression microarray experiment at 6 h after Cu^{2+} addition (WT_pVZ: black;
682 IsaR1OE: blue) and the iron depletion microarray experiment at 48 h after DFB addition
683 (WT: grey; Δ*isaR1*: red) are shown as dots (probe position) connected by lines. The
684 numerical values for the microarray data are shown in log_2 scale (left y-axis). The lower
685 portion displays the sequence of the *sufB* upstream region ending with the start codon,
686 including both *sufB* TSSs. The proposed palindromic SufR binding sites [34] are
687 marked with arrows and are in uppercase. The *sufZ* sequence is boxed, and the
688 predicted *sufB*-IsaR1 interaction is highlighted in grey.
689 **(B)** The generation of SufZ strictly depends on the presence of IsaR1. Time course of
690 iron stress for WT, IsaR1OE and Δ*isaR1* strains in the presence of copper ions,
691 inducing IsaR1 expression in IsaR1OE. Upper portion: Northern hybridization with a
692 probe to SufZ, lower portion: hybridization with a probe to IsaR1. Note the lack of
693 detectable SufZ accumulation in ΔIsaR1.
694 **(C)** Verification of the IsaR1–SufZ/*sufB* interaction in the sGFP reporter assay. Density
695 plots of representative flow cytometer measurements (50,000 events each) for *E. coli*
696 strains harboring different plasmid combinations. Left box: strain with no GFP (black),
697 translational fusion of WT *sufB*-UTR with sGFP in the presence of the control plasmid
698 pJV300 (red), the presence of IsaR1 (yellow), or IsaR1 with the two point mutations
699 shown in panel E (blue). Right box: strain with no GFP (black), translational fusion of

*sufB**-UTR containing point mutations with sGFP in the presence of the control plasmid pJV300 (red), the complementary IsaR1* version (yellow), or WT IsaR1 (blue). Inset in left box: Fold repressions of the GFP fluorescence from the WT *sufB*-sGFP fusion with IsaR1 (*sufB* + isaR1), with IsaR1* (*sufB* + IsaR1*) and from the *sufB**-sGFP fusion in the presence of IsaR1 (*sufB** + IsaR1) or the mutated IsaR1 version (*sufB** + IsaR1*). The fold repression and the respective error were calculated from 6 independent clones for each strain (details in **Figure S4A** and **S5A**).

(D) Predicted interaction between the SufZ/*sufB* 5′ UTR and IsaR1 (for comparison to other interaction sites, see **Figure S7**). The seed region of interaction is boxed in orange, start codon and ribosome binding site in black. Point mutations are indicated by stars and orange letters.

(E) Expression of the *sufBCDS* operon and *sufR* mRNAs and of IsaR1 during the iron depletion time course in WT and Δ*isaR1* (black, upper part). The error bars are calculated from 2 independent microarray experiments for each time point. In the lower portion, the respective protein expression levels from the SRM experiment are shown (red). The error bars are calculated from 2 independent experiments for each time point (x-axis: time after DFB addition, in hours).

Figure 7. Model of IsaR1 function. General overview of the IsaR1 regulon and its connections to FurA and SufR in the iron depletion stress response. The expression of IsaR1 is controlled by FurA (**Figure S2**). High confidence targets are in bold. Black lines indicate verified or proposed (broken) direct post-transcriptional regulation by IsaR1. Blue lines indicate regulatory relationships indirectly affected by IsaR1. Grey lines indicate regulatory events independent of IsaR1.

The source of evidence for IsaR1 targets is indicated by the filled circles for respective genes or gene products; for the underlying details please see **Table S3**. In each of

these panels, top left: evidence from IntaRNA or comparative CopraRNA target prediction (**Figure 3A**). Top right: pulse expression microarray (**Figure 4**) and iron depletion microarray evidence (**Figure 2, 3B**). Bottom left: Western blot (PetF, PetA, PsaB (**Figure S6**) or pulse IsaR1 overexpression SRM proteomic evidence (absolute $\log_2$ FC 96 h after induction ≥0.8). Bottom right: Evidence from the GFP-reporter assay in the *E. coli* system ($\log_2$ fold repression by IsaR1 ≥1.5).

STAR METHODS SECTION

CONTACT FOR REAGENT AND RESOURCE SHARING

Further information and requests for resources and reagents should be directed to and will be fulfilled by the Lead Contact, Wolfgang R. Hess (wolfgang.hess@biologie.uni-freiburg.de).

EXPERIMENTAL MODEL AND SUBJECT DETAILS

Culture Conditions and Mutagenesis

We used the *Synechocystis* 6803 substrain PCC-M [40], cultured on BG-11 medium [41] with reduced iron concentrations [42], supplemented by 0.75% (w/v) agar (Bacto agar, Difco) for plating. Liquid cultures were grown in BG-11 medium containing 10 mM TES buffer (pH 8.0) under continuous illumination with white light of 50 µmol photons m^{-2} s^{-1} at 30 °C. Iron starvation was triggered by addition of the chelator DFB (Sigma-Aldrich) at a final concentration of 100 µM. The choice of DFB was motivated by its superior effectiveness compared with the alternative media exchange method and other chelating agents [13]. Samples were taken before the induction of iron depletion, as well as at 3, 12, 24, 48, and 72h after induction of iron depletion. Media for mutant strains were supplemented with 40 µg mL^{-1} kanamycin or 2 µg mL^{-1} gentamicin separately, or in combination. Copper-free BG11 medium was used for cultivation of the inducible overexpression mutant IsaR1OE and the respective control strain. For induction of the *petE* promoter $CuSO_4$ was added to a final concentration of 2 µM. Different growth conditions are indicated in the respective figures.

The IsaR1OE strain was constructed by inserting *isaR1* between the P_{petE} promoter for controlled expression and the *oop* terminator for the termination of transcription. To obtain the Δ*isaR1* strain, a kanamycin resistance cassette was inserted using homologous recombination to disrupt the *isaR1* gene.

METHOD DETAILS

Spectroscopy

The absorption spectra of whole cells were recorded using an UV-2401 PC spectrophotometer (Shimadzu). For measurement of the 77K fluorescence emission spectra, the cyanobacterial cultures were adjusted to the same chlorophyll concentration (7.5 µg Chl a/mL). The samples with intact cells were rapidly frozen in liquid nitrogen. The spectra were measured using a USB4000-FL-450 spectrofluorometer (Ocean Optics) with 440 nm excitation (10 nm width). The spectra were normalized at 726 nm.

Photosynthetic electron transfer

The P700 and Chl a fluorescence measurements were recorded with a Dual-PAM-100 pulse amplitude modulated fluorometer (Walz, Germany). The effective yield of PSI, Y(I), was calculated as $Y(I) = (P'_m - P)/ P_m$, where P'_m represents the maximal change of the P700 signal under actinic light upon application of a saturating pulse (5,000 µmol photons m^{-2} s^{-1}, 300 ms), and P indicates the fully reduced form of P700. P_m is the maximal change of the P700 signal upon transformation of P700 from the fully reduced to the fully oxidized state, achieved by the application of a saturation pulse after pre-illumination with far-red light (720 nm, 75 W/m^{-2}). The acceptor side limitation Y(NA) was calculated as $Y(NA) = (P_m - P'_m) / P_m$. It indicates the fraction of P700 that cannot be oxidized by a saturating pulse because of the shortage of oxidized acceptors. The maximum quantum yield of PSII (F_v/F_m) was calculated as $(F_m-F_0)/F_m$, where F_m is the maximum fluorescence level measured in the presence of 20 µM DCMU, and F_0 is the fluorescence level after turning on the measurement light. The

784 fluorescence was recorded from dark-adapted cells upon the application of 200 µmol
785 photons m^{-2} s^{-1} red actinic light for 1 min.
786
787 **Plasmids and Mutagenesis**
788 The IsaR1OE strain was constructed as follows: The pJet1.2 plasmid was digested
789 with *Pvu*II and *Swa*I restriction enzymes, and the 2,118 nt fragment was
790 dephosphorylated and used for blunt-end ligation with the P*petE* fragment amplified
791 from *Synechocystis* 6803 using primers pPetEfw and pPetErv (sequences see below).
792 Plasmid pJet_PetE contained the *petE* promoter for the controlled expression of
793 sRNAs and the *oop* terminator for the termination of transcription. The *isaR1* fragment
794 was amplified with IsaR1_for and IsaR1_ecoRI_rev primers, and digested with *Eco*RI
795 resulting in blunt ended 5' and an *Eco*RI 3' sticky end. The fragment was then ligated
796 to the pJet_PetE plasmid and digested with *Pvu*II and *Eco*RI. The resulting P*petE-*
797 *isaR1* construct was excised by *Hind*III/*Xho*I and inserted into plasmid pVZ322. The
798 resulting plasmid, pVZ_pPetE_IsaR1, was transferred to WT cells by conjugation and
799 exconjugants were selected on BG11 agar plates containing 2 µg mL^{-1} gentamicin.
800 The same plasmid was used to create the strain IsaR1comp, by conjugation into strain
801 Δ*isaR1*. A plasmid containing only the regulatory regions was generated to obtain
802 isogenic control strains, WT_pVZ__pPetE and Δ*isaR1*_pVZ.
803 For construction of the Δ*isaR1* strain, regions up- and downstream of *isaR1*
804 were amplified with primer combinations Syr22Kno_rechte_Fl_AgeI_fw and Syr22-
805 Kno_rechte_Fl_rev (for the upstream homologous flank) and Syr22-
806 Kno_linke_Fl_FseI_rev and Syr22-Kno_linke_Fl_fw (for the downstream homologous
807 flank; see below for primer sequences). The flank upstream was ligated into vector
808 pJET1.2, afterwards the downstream flank was ligated into this newly created vector.
809 Restriction enzymes *Fse*I and *Age*I were used to open the vector and insert the

kanamycin resistance cassette. Transformants were selected on 50 µg mL^{-1} kanamycin.

Oligonucleotides used in this study.

Name	**Sequence (5'- 3')**	**Purpose**
pPetEfw	taaAAGCTTgaagggatagcaagctaatttttatgacgg	P_{petE} fragment
pPetErv	taactcgagAATAAAAAACGCCCGGCGGCAACCGAGCGAATTCCAAGAGTATTcagCTGCCCATGGTATCACAATGTTTGACA	P_{petE} fragment
IsaR1_for	ACAGTGTTCTCTTCTCAAGGATTCAG	IsaR1 fragment
IsaR1_ecoRI_rev	taagaattcCTAATCAGTTTAAGGTTTTGCCGCC	IsaR1 fragment
Syr22Kno_rechte_FI_AgeI_fw	ACCGGTCAGATTACTGCAAATTATTGTCAATATTG	Δ*isaR1*
Syr22-Kno_rechte_FI_rev	CCTAAACCTTTCCGTGAATTGC	Δ*isaR1*
Syr22-Kno_linke_FI_FseI_rev	GGCCGGCCCGTGTCCGTTGTTAACTTTTTGC	Δ*isaR1*
Syr22-Kno_linke_FI_fw	GAGAATGTTGGCGGTCATCAC	Δ*isaR1*
sufZ_for	GATTAAAACAACTTACCTGTTGTTTTAG	Northern blot – SufZ and SufB
T7_sufZ_sufB_rv	TAATACGACTCACTATAGGGCGCACCACGTCTTCACTC	Northern blot – SufZ and SufB
Syr22-T7-fw	TAATACGACTCACTATAGGGCAAAAAGTTAACAACGGACACG	Northern blot IsaR1
Syr22-rev	AGTGTTCTCTTCTCAAGGATTCAG	Northern blot IsaR1
Syr22-*Kpn*I-fw	GGTACCTCCCGATTTACTCCAGCAGGC	*luxAB* assay
Syr22-*Kpn*I-rev	GGTACCCTACTGAATCCTTGAGAAGAGAAC	*luxAB* assay
isiA-fw*Age*I	ACCGGTCATTGGATTAAAGCCATGAGTTG	*luxAB* assay
isiA-rev*Fse*I	GGCCGGCCGAATCTTTAGCACTTACTCCCG	*luxAB* assay
Syr22_5_phos	ACAGTGTTCTCTTCTCAAGGATTCAG	pIsaR1
Syr22_3_xbaI	GTTTTTTCTAGACTAATCAGTTTAAGGTTTTGCCGCC	pIsaR1
IsaR1_GFP_m1_fw	ACAGTtaTCTCTTCTCAAGGATTCAGTAGGG	pIsaR1*
IsaR1_GFP_m1_rv	GAAGAGAtaACTGTGTGCTCAGTATCTTGTTATC	pIsaR1*
IsaR1_GFP_m2_fw	ACAGTGTaCcgTTCTCAAGGATTCAGTAG	pIsaR1**
IsaR1_GFP_m2_rv	TTGAGAAcgGtACACTGTGTGCTCAGTAT	pIsaR1**
ycf24_5_NsiI	TTAATGCATACAACCCCCATGCTAAGCAGG	pXG10_sufB
ycf24_3_NheI	TTAGCTAGCGGTGACAAAGCCATATTTGTAGGG	pXG10_sufB
ycf24_m1_fw	CCGGAGAtaACTGCATTCGATGAGTTC	pXG10_sufB*
ycf24_m1_rv	ATGCAGTtaTCTCCGGGGAATTCAGATAG	pXG10_sufB*
petJ_5_NsiI	TTAATGCATCTTCGCGTCTTGAAGACTTTATCCT	pXG10_petJ
petJ_3_NheI	TTAGCTAGCAGCTTGGTTGAATAATTTAAACATTAGTTCTC	pXG10_petJ
petF_5_NsiI	TTAATGCATAGTTAAGTTTTTTGAAGTAGCTCGATCTG	pXG10_petF
petF_3_NheI	TTAGCTAGCGATGGAACTTTCACCATCGGGG	pXG10_petF
sodB_5_NsiI	TTAATGCATATGGAATCCCCTATTGAGTAGAGAATT	pXG10_sodB
sodB_3_NheI	TTAGCTAGCCTCCAGGGTGCTTTTGGAAATG	pXG10_sodB

sodB_m2_fw	TTGAGTAcgGtATTTAAATTTAAATGGCTTACGCACT	pXG10_sodB**
sodB_m2_rv	TTTAAATaCcgTACTCAATAGGGGATTCCAT	pXG10_sodB**
ilvD_5_NsiI	TTAATGCATAAGCATAGATTCGCTACGAGACAG	pXG10_ilvD
ilvD_3_NheI	TTAGCTAGCATCGCCAAAACCAACGGCCCG	pXG10_ilvD
psaA_5_NsiI	TTAATGCATATGTTTGCTGAAAACGCCTATCTGTG	pXG10_psaA
psaA_3_NheI	TTAGCTAGCCTTGCCCCACTTCTCGAAGGAAG	pXG10_psaA
slr0665_5_NsiI	TTAATGCATATTCACCGTTGACCATGAACTAATATTG	pXG10_acnB
slr0665_3_NheI	TTAGCTAGCCAGTTCACATAGTTCAGTAGTCTGC	pXG10_acnB
chlN_5_NsiI	TTAATGCATTTACGATTTACCAACGATCAAGTTATTG	pXG30_chlN
chlN_5_NheII	TTAGCTAGCTTGATAAAGCCAAGATACGCAACTAATG	pXG30_chlN
hemA_5_NsiI	TTAATGCATATTAGAGAAACTTGTTTAACAAAAAACGTCG	pXG10_hemA
hemA_3_NheI	TTAGCTAGCCCGCAGATGGGTTAGCGCTTC	pXG10_hemA
psaC_5_NsiI	TTAATGCATAATCCTGACAATATTATTTTTTTCGACTTTACG	pXG10_psaC
psaC_3_NheI	TTAGCTAGCGGGCACCATTTCTAGAACATCGA	pXG10_psaC
petD_5_NsiI	TTAATGCATCACACCTTCGTGCTTCCCTG	pXG30_petD
petD_3_NheI	TTAGCTAGCGGGCTCACCATAATAGTTGTGAC	pXG30_petD
petA_5_NsiI	TTAATGCATAGCACCTGGACCGAAACCGA	pXG30_petA
petA_3_NheI	TTAGCTAGCGACGCTGACTGTGGCGATC	pXG30_petA
nifJ_5_NsiI	TTAATGCATAAGACCCAGAGAGAACGCCATG	pXG10_nifJ
nifJ_3_NheI	TTAGCTAGCGGGATAAATGGCAATCACTTCACTG	pXG10_nifJ
sdhA_5_NsiI	TTAATGCATAGGCAGGCCCCTAGGGATT	pXG10_sdhA
sdhA_3_NheI	TTAGCTAGCTTTGGTATCAGGGGCCAGACG	pXG10_sdhA
sll0041_pixJ_5_NsiI	GTTTTTATGCATCGTCTGATGACTACTCCCCGG	pXG30_pixJ
sll0041_pixJ_3_NheI	GTTTTTGCTAGCTACCTCACTTTTATCCTCTCCATCG	pXG30_pixJ
cph2_5_NsiI	GTTTTTATGCAT ACAATTTAGCTGAGTAAATTTTTTACATTTACTTTATTC	pXG10_cph2
cph2_3_NheI	GTTTTTGCTAGCGAGGGTTTCCCGTAAAGTCAAAGC	pXG10_cph2
petB_5_NsiI	GTTTTTATGCATGAGTAGTTCTCATTTTTGCCAAGTTTGG	pXG10_petB
petB_3_NheI	GTTTTTGCTAGCAACGTATTTGCTGGCAATGTCATC	pXG10_petB
slr1593_5_NsiI	GTTTTTATGCATAGAAAATCTTAAGGTTTTCTCCTCCCC	pXG10_slr1593
slr1593_3_NheI	GTTTTTGCTAGCAGAACTATTGCTCTCCTCTGGG	pXG10_slr1593
psbE_5_NsiI	TTAATGCATACTTGCTTTGCATTTGTCAGTCAATG	pXG10_psbE
psbE_3_NheI	TTAGCTAGCACCAGCAATAAACAACATCGGGATG	pXG10_psbE
fumC_5_NsiI	TTAATGCATCTGCGCCATTTAGACCGGG	pXG30_fumC
fumC_3_NheI	TTAGCTAGCGGAACGTTGGGTTTGCGCTC	pXG30_fumC
slr0857_5_NsiI	GTTTTTATGCATAACTATGTTATCGAGAAAGAAACCGGG	pXG30_ISY100
slr0857_3_NheI	GTTTTTGCTAGC AGATTCATCTATGTAAACTATAGCTTGACTAC	pXG30_ISY100
slr0473_5_NsiI	GTTTTTATGCATACCCAGAATATTTGGCCGTTATCGC	pXG10_cph1
slr0473_3_NheI	GTTTTTGCTAGCACCGTGGGGCTGAATCAGGTG	pXG10_cph1
NdeI-FurA-F	AACATATGTCCTACACCGCCGAT	FurA expression in *E. coli*
XhoI-FurA-R	AACTCGAGCTAGGCCAAGGAAATACT	FurA expression in *E. coli*
PisaR1-F	TTGCCCCACTCCATTTGG	gels shift
PisaR1-R	GCCGCCAAAAAAACAGGG	gels shift

IsaR1-sub-F	GTCTCCAACAATAccccccccAccccccccGTAATCTGTATAGTG ATTTCACAGTG	mutagenesis of P_{isaR1}
IsaR1-sub-R	GGGGGTATTGTTGGAGACATTCTCCG	mutagenesis of P_{isaR1}

813

814 **Reporter Gene Assays**

815 For the promoter assays the upstream sequences of *isaR1* (-131 to +29
816 referring to the first transcribed nucleotide +1 [43] and *isiA* (-295 to +38) were
817 transcriptionally fused to *luxAB* genes. The reporter constructs were generated by PCR
818 amplification using the oligonucleotides isiA-fwAgeI/isiA-rev/FseI (P*isiA*) and
819 SyR22_KpnI_fw/rev (P*isaR1*) followed by digestion with *Kpn*I and *Age*I/*Fse*I,
820 respectively. The products were cloned into the reporter plasmid pILA [21], which was
821 then used to transform a *Synechocystis* strain expressing *luxCDE* genes to provide the
822 substrate for the luciferase reaction. Bioluminescence was measured as described
823 [44]. As negative control a strain harboring promoterless *luxAB* genes was used.

824

825 **Construction of *E. coli* Strains Expressing His-tagged FurA**

826 The coding region of *furA* (*sll0567*) was amplified by PCR using the primers NdeI-FurA-
827 F and XhoI-FurA-R, and cloned into pT7Blue T-vector (Novagen). The PCR fragments
828 were *Nde*I/*Xho*I excised from pT7Blue and subcloned into the same restriction sites in
829 vector pET28a (Novagen) to express proteins with an N-terminal 6xHis-tag. The
830 expression construct was transformed into Origami2 (DE3) competent cells (Novagen).

831

832 **Expression and purification of recombinant FurA**

833 *E. coli* Origami2 (DE3) strains harboring the FurA expression construct, were
834 precultured in 2 mL TB medium containing kanamycin at 37°C overnight. The
835 preculture was seeded into 500 mL 2×YT medium. FurA expression was induced in
836 midlog cultures grown overnight at 15°C with 100 µM IPTG.

837 Purification of 6xHis-FurA protein was performed using an immobilized metal
838 affinity-chromatography (IMAC) resin charged with cobalt. Washing was performed
839 with phosphate buffer and protein was eluted with 300 mM imidazole. All steps were
840 performed at 4°C on ice. For further processing, the protein was desalted and
841 concentrations were determined with the Bradford assay.
842
843 **Promoter Gel Shift Experiments**
844 The *isaR1* promoter fragment (from nucleotide position 3,164,543 to 3,164,317
845 according to the numbering in CyanoBase) was PCR-amplified from genomic DNA
846 using primer pairs PisaR1-F and PisaR1-R, and cloned into the pT7Blue T-vector
847 (Novagen). Point mutations were introduced using the Prime STAR Mutagenesis Kit
848 (Takara) using primer pairs IsaR1-sub-F and IsaR1-sub-R. P*isaR1* and P*isaR1*-sub
849 fragments were PCR amplified from these two vectors using primer pairs PisaR1-F
850 and PisaR1-R.
851 For digoxigenin (DIG) labeling, 3.85 pmol of PCR product (here approx. 1.5-2.5
852 µL) was filled up to 10 µL with H_2O and the following components were added: 4 µL
853 each of 5x buffer and of $CoCl_2$, 1 µL each of DIG-ddUTP and of terminal transferase.
854 The labeling mixture was incubated at 37°C for 15 min, then 2 µL of the EDTA stop
855 solution and 3 µL of H_2O were added. To avoid precipitation, DIG-labeled probe was
856 buffer-exchanged into Tris-borate buffer using Zeba Desalt Spin Columns (Thermo
857 Scientific). Binding reactions between FurA and the DIG-labeled probe were performed
858 according to the protocol of Roche's „DIG gel shift kit, 2nd generation" and literature
859 [45]. Samples were separated on native-polyacrylamide (4%) gels and blotted
860 overnight on Hybond N+ nylon membrane (GE Healthcare). DIG-labelled fragments
861 were detected with anti-DIG serum and CDP-Star.
862

863 **RNA Preparation and Microarray Analysis**

864 *Synechocystis* 6803 liquid cultures were collected by quenching on ice and immediate
865 centrifugation at 4 °C. The RNA was isolated as previously described [46] with an
866 additional phenol/chloroform/isoamyl alcohol (25:24:1 v/v) extraction preceding the
867 RNA precipitation. Templates for probe generation were prepared using PCR. For
868 microarray analysis, 2 µg of DNA-free total RNA was labeled, and 1.65 µg of RNA was
869 used for hybridization. The raw fluorescence data had the normexp background
870 subtracted, and were quantile normalized. The subsequent statistical analysis of fold
871 changes and pre-processing was performed using limma [47]. Transcripts with an
872 absolute $\log_2$-fold change of ≥0.9 and an adjusted p-value ≤0.05 between IsaR1OE
873 and the control strain were taken as potential targets. Additionally, transcripts that
874 showed a significantly different response to the copper addition were included (i.e.,
875 |(IsaR1OE 6h – IsaR1OE 0h) – (control 6h – control 0h)| > 0.9, adj. p-value ≤ 0.05)
876 (**Figure 4**). Furthermore, we excluded all differentially expressed genes from the 0 h
877 time point (IsaR1OE 0h – control 0h <0.8) to single out targets that responded to IsaR1
878 overexpression. If transcripts were within the top-100 list predicted by CopraRNA or
879 IntaRNA, we lowered the $\log_2$-fold change threshold to 0.5. The full dataset is
880 accessible from the GEO database under accession number GSE87496.

881

882 **Target Verification with a Heterologous Reporter System**

883 We used the sGFP plasmid system [26] to test 22 mRNAs that were suggested as
884 direct targets of IsaR1 by prediction and microarray. We started from single bacterial
885 colonies and measured fluorescence directly using an Accuri C6 flow cytometer (BD
886 Biosciences). The list of plasmids is given below. For each clone, the fluorescence of
887 50,000 events was collected. The events were individually gated for each well to retain
888 the events with a fluorescence lower than or equal to the mean of all fluorescence

values plus four times the standard deviation. The mean of the gated events was averaged for 6 independent biological replicates. The fold repression was calculated as the ratio of the mean sGFP fluorescence of the respective translational 5'UTR–sGFP fusion in the presence of the control plasmid pJV300 and a plasmid for the overexpression of the respective sRNA, after the subtraction of the background fluorescence. The background fluorescence was measured with the control plasmids pXG-0 (with a luciferase gene instead of GFP) and pJV300, from which a short nonsense transcript is transcribed instead of a specific sRNA. The error of the fold repression was calculated considering error propagation under the assumption that the values could be correlated. A fold repression of at least 1.5 was detected for 10 targets (*sufB, sodB clhN, petF, psbE, psaA, hemA, petJ, ilvD* and *acnB*). Two targets showed no effect in the heterologous system (*psaC* and *petD*). The remaining 10 constructs had fluorescence at background or slightly above the control plasmid background levels, which made it impossible to conclude a regulatory function of IsaR1. Five of these candidates showed clear repression but with high uncertainty (*cph1, ISY100, sdhA, petB, nifJ*). In the case of *hemA*, the background was not subtracted for calculation of the fold repression. The raw fluorescence data for all UTRs tested are shown in **Figure S4**.

List of plasmids used in this study:

Name	**Origin, marker**	**Comment**	**Reference**
pJet_PetE	Amp^R	Plasmid for controlled expression of sRNAs directed by the *petE* promoter (P*petE*; activated by addition of Cu^{2+}) with no additional nucleotides at the 5' end. The oop terminator ensures reliable termination of the overexpressed gene. Directed insertion of the gene of interest via restriction sites for *Pvu*II and *Eco*RI between promoter and terminator. The gene of interest should be blunt ended at 5' and with an *Eco*RI 3' sticky end.	This study
pVZ_pPetE_ IsaR1	Gen^R	Plasmid used for conjugation in *Synechocystis* for generation of IsaR1OE mutant (WT background) and IsaR1comp mutant (Δ*isaR1* background). For	This study

		inducible expression of IsaR1 under the control of PpetE.	
pVZ_pPetE	Gen^R	For generation of isogenic control strains WT_pVZ and Δ*isaR1*_pVZ.	This study
pIsaR1	ColE1, Amp^R	IsaR1 expression plasmid	This study
pIsaR1*	ColE1, Amp^R	Derivative of pIsaR1	This study
pIsaR1**	ColE1, Amp^R	Derivative of pIsaR1	This study
pXG10_sufB	pSC101*, Cm^R	sfGFP reporter plasmid. Carries the *SufB* 5'UTR and the first 60nt of the coding sequence	This study
pXG10_sufB*	pSC101*, Cm^R	Derivative of pXG10_sufB	This study
pXG10_petJ	pSC101*, Cm^R	sfGFP reporter plasmid. Carries the *petJ* 5'UTR and the first 24nt of the coding sequence	This study
pXG10_petF	pSC101*, Cm^R	sfGFP reporter plasmid. Carries the *petF* 5'UTR and the first 51nt of the coding sequence	This study
pXG10_sodB	pSC101*, Cm^R	sfGFP reporter plasmid. Carries the *sodB* 5'UTR and the first 75nt of the coding sequence	This study
pXG10_sodB**	pSC101*, Cm^R	Derivative of pXG10_sodB	This study
pXG10_ilvD	pSC101*, Cm^R	sfGFP reporter plasmid. Carries the *ilvD* 5'UTR and the first 90nt of the coding sequence	This study
pXG10_psaA	pSC101*, Cm^R	sfGFP reporter plasmid. Carries the *psaA* 5'UTR and the first 90nt of the coding sequence	This study
pXG10_acnB	pSC101*, Cm^R	sfGFP reporter plasmid. Carries the *acnB* 5'UTR and the first 99nt of the coding sequence	This study
pXG30_chlN	pSC101*, Cm^R	sfGFP reporter plasmid. Carries the last 102 nt of *ssr1251* the *ssr1251-chlN* intergenic region and the first 102 nt of the *chlN* coding sequence	[27]
pXG10_hemA	pSC101*, Cm^R	sfGFP reporter plasmid. Carries the *hemA* 5'UTR and the first 108 nt of the coding sequence	[27]
pXG10_psaC	pSC101*, Cm^R	sfGFP reporter plasmid. Carries the *psaC* 5'UTR and the first 90 nt of the coding sequence	This study
pXG30_petD	pSC101*, Cm^R	sfGFP reporter plasmid. Carries the last 90 nt of *slr0342* the *slr0342-petD* intergenic region and the first 90 nt of the *petD* coding sequence	This study
pXG30_petA	pSC101*, Cm^R	sfGFP reporter plasmid. Carries the last 54 nt of *petC1* the *petC1-petA* intergenic region and the first 90 nt of the *petA* coding sequence	This study
pXG10_nifJ	pSC101*, Cm^R	sfGFP reporter plasmid. Carries the *nifJ* 5'UTR and the first 90 nt of the coding sequence	This study
pXG10_sdhA	pSC101*, Cm^R	sfGFP reporter plasmid. Carries the *sdhA* 5'UTR and the first 90 nt of the coding sequence	This study
pXG30_pixJ	pSC101*, Cm^R	sfGFP reporter plasmid. Carries the last 36 nt of *pixI* the *pixI-pixJ* intergenic region and the first 177 nt of the *pixJ* coding sequence	This study
pXG10_cph2	pSC101*, Cm^R	sfGFP reporter plasmid. Carries the *cph2* 5'UTR and the first 84 nt of the coding sequence	This study
pXG10_petB	pSC101*, Cm^R	sfGFP reporter plasmid. Carries the *petB* 5'UTR and the first 99 nt of the coding sequence	This study
pXG10_slr1593	pSC101*, Cm^R	sfGFP reporter plasmid. Carries the *slr1593* 5'UTR and the first 99 nt of the coding sequence	This study
pXG10_psbE	pSC101*, Cm^R	sfGFP reporter plasmid. Carries the *psbE* 5'UTR and the first 102 nt of the coding sequence	This study
pXG30_fumC	pSC101*, Cm^R	sfGFP reporter plasmid. Carries the last 96 nt of *murA* the *murA-fumC* intergenic region and the first 90 nt of the *fumC* coding sequence	This study
pXG30_ISY100	pSC101*, Cm^R	sfGFP reporter plasmid. Carries the last 57 nt of *slr0856* and the first 60 nt of the *slr0857 (ISY100)* coding sequence	This study
pXG10_cph1	pSC101*, Cm^R	sfGFP reporter plasmid. Carries the *cph1* 5'UTR and the first 90 nt of the coding sequence	This study

908

909 **Protein Extraction and Western Blots**

910 The protein extraction followed the protocol described in Vuorijoki et al. [10]. Briefly,
911 proteins were extracted as a whole cell lysate in extraction buffer containing 0.1 M
912 ammonium bicarbonate (NH_4HCO_3), 8 M urea, 0.1% (w/v) Rapigest SF (Waters
913 Corporation, Milford, MA) and 0.2 mM PMSF. The cells were disrupted in a bead beater
914 (Mini-Bead-Beater-8, Unigenetics Instruments Pvt. Ltd., India), and the protein
915 concentration was determined using the Bradford assay. For Western blots, protein
916 samples were separated on a 12% SDS-PAGE gel and blotted to PVDF membranes
917 (Immobilon-P; Millipore). Protein-specific antibodies were used for the
918 immunodetection of proteins of interest.

919

920 **SRM Triple Quadrupole Liquid Chromatography Mass Spectrometry**

921 Protein extracts were reduced with 5 mM dithiothreitol (DTT; Sigma) and alkylated with
922 10 mM iodoacetamide (IAA; Sigma), followed by o/n acetone:ethanol precipitation at -
923 20 °C. The resulting protein pellets were digested o/n in 50 mM NH_4HCO_3 and 5 %
924 (v/v) acetonitrile (ACN) buffer with two additions of trypsin (Sequence grade Modified,
925 Promega, Madison, WI, USA) at a 1:100 (w/w; trypsin:protein) ratio. The samples were
926 desalted by solid-phase extraction using a 4 mm/1 ml extraction disk cartridge (Empore
927 C18-SD, 3M).

928 The SRM assays were performed using a TSQ Vantage QQQ mass
929 spectrometer (Thermo Scientific) equipped with a nanoelectrospray ionization source.
930 The desalted peptides were separated using a nanoflow HPLC system (EasyNanoLC
931 1000; Thermo Scientific). One hundred-fifty ng of each unfractionated biological
932 triplicate was injected, including the spiked-in iRT peptides (Biognosys). A 60 min non-
933 linear gradient (5-20% B in 35 min; 20–35% B in 50 min; B=ACN:water, 98:5) was

applied at a 300 nL/ min flow rate. Once the peptides were eluted and ionized, they were analyzed using the QQQ-MS, operated in SRM mode, as described [10]. To maintain high sensitivity in SRM measurement, scheduled assays with a 5 min retention time for each peptide were applied, resulting in a 2.5 s cycle and >30 ms dwell time. The protein targets and respective SRM assay parameters were selected from a public dataset, available from Panorama Public (https://panoramaweb.org/labkey/Vuorijoki_et_al_2015.url) [10]. Forty-two proteins with 107 proteotypic peptides (PTPs) were quantified in the Δi*saR* analysis and 41 proteins with 104 PTPs in the IsaR1OE analysis. The data were processed using Skyline [48], and MSstats (3.1.4) [49] was used for relative quantification. Two endogenous peptides (YEAQNIEELTAEK and TPLFNIK) of the drug sensory protein A (*dspA; sll0698*) were used to normalize the data with a global standard normalization method. The SRM result files are available from Panorama Public [50] in Skyline format (https://panoramaweb.org/labkey/IsaR1.url), and the raw data can be accessed in the PeptidesAtlas SRM Experiment Library (PASSEL).

QUANTIFICATION AND STATISTICAL ANALYSIS

Computational Prediction of IsaR1 Targets

IsaR1 target prediction was conducted using CopraRNA [24] on webserver version 2.0.3.2 with standard parameters. The 20 organisms used are highlighted in **Figure S1A**. An alignment of the respective IsaR1 sequences is shown in **Figure S1B**. The FASTA sequences of the IsaR1 homologs and the Refseq IDs of the 20 organisms are provided below. The downloadable results of the CopraRNA prediction (**Data S2**) include the individual whole-genome target predictions for all organisms. The respective IntaRNA prediction for *Synechocystis* 6803 (**Data S2**) was used for comparison with the microarray results.

IsaR1 homologs used for the CopraRNA target prediction:

>NC_000911
ACAGTGTTCTCTTCTCAAGGATTCAGTAGGGGGTGGCTCGGCGATCGAGTGCTCCCTGTTTTTTTGGC
>NC_011726
TTGTGTTCTCCTCTCAAGGATCGGCAGGTGGAATCGTTCAGGACAGACGGTTCCCCTCTTTTTTGT
>NC_011884
CAGTGTTCTCCTCTCTGAGGAATAGGCAGGTGGGGTCAGGAAGCGCGATGCCGATCGGCCCCCTGTTT
>NZ_CP007542
TAGTGTTCTCTTCTCAAGGATTCAGTAGGGGGTGGCTCGGCGATCGGGTGCTCCCTGTTTTTTTTGC
>NC_010628
CAGTGTTCTCCTCTCTTTTAAGGATCGGCAGACGGGATTAGCCAGCAGTAGCAGGCTCGTCCCTCTTTTT
>NC_014248
ACAGTGTTCTCCTCTCTTTAAAGGATCGGCAGACGGGATTGGCCAGCGGTAGCAGGCTTATCCCTCTTTTT
>NC_019780
CAGTGTTCTCCTCTCGTTAAGAAGCAAGAAGCAGGTGGGGTAAGTCCGACCCCATCTCTTTTTTTTTGCGC
>NC_019771
TAGTGTTCTCCTCTCTTTAAAGGATCGGCAGACGGGATAGCCAGCAGCAGCAGGTTTGTCCCTCTTTTTT
>NC_003272
CAGTGTTCTCCTCTCTTTAAGGATCGGCAGACGGGATTAGTCGGCGGTAGCAGGCTCATCCCTCTTTTT
>NC_019689
AAGTGTTCTCCTCTCAAGGATCGGCAGGTGGGACCGCTAAGTCAGTATAAGGGCGGCTCTCCTGT
>NC_014501
ACAGTGTTCTCCTCTCAAGGATCGGCAGGTGGGACCGCTTGGCAGTCAATAAATGCGGCTCCCCTGT
>NC_009925
ATGTGTTCTCCTCTCAGAGGATTCGGCAGGTGGGGCCAAGGCGTTAGCGCAGCTTGGTTCCATTTTTT
>NC_010547
AAGTGTTCTCCTCTCAAGGATGGATCGGCAGGTGGAATCGTTCAGCAACACAGAGACGGTTCCCCTATTT
>NC_019748
AGTGTTCTTCTCTCAAGGAATCGGCAGGCGGGATCGCGAGTCATTAAAAAAGCGACTCCCCTGTTTTT
>NC_019745
CAGTGTTCTCCTCTCTTTTAAAGATCGGCAGACGGGGTTGGTCAGCAGTAGCAGACTGATCCCTATTTTT
>NC_019695
AAGTGTTCTCCTCTCTTTAAGGATCGGCAGACGGGATTGGTCAGCAAGTGCGGCTAATCCCTATTTTTT
>NZ_CM001793
TAGTGTTCTCCTCTCTTTAAGGATCGGCAGACGGGATTAGCCAGCAGCAGCAGGCTTGTCCCTCTTTTT
>NC_019678
CAGTGTTCTCCTCTCTTTAAGGAACGGCAGGCGGGATTGGTCAGCAGTTGCGGACTTGTCCCTCTTTTT
>NC_019751
CAGTGTTCTCCTCTCTTTAAGGATCGGCAGACGGGATTAGCCAGCTTCAGCAGGCAGTCCCTCTTTTTT
>NC_010296
AGTGTTCTCCTCTTAAGGATCGGCAGTGGAACCGCGCGGCAGTCTCTAACAATGCGGTTCCCATTTTTTTT

DATA AND SOFTWARE AVAILABILITY

Synechocystis 6803 IsaR1is located from positions 3164387-3164320 on the reverse complementary strand (GenBank file NC_000911.1). Microarray data have been deposited in the GEO database (accession number GSE87496) and SRM data in Panorama Public and PASSEL at http://www.peptideatlas.org/PASS/PASS00939.

Table S1. Differentially abundant transcripts in Δ*isaR1* and WT after 48 h of iron starvation, arranged according to operons and encoded functions. Related to **Figure 2**.

Table S2. Differentially abundant proteins in IsaR1OE compared to WT in a time course 0, 24 and 96 h after induction (Figure 3B), arranged according to operons and encoded functions.

Table S3. Additional information to the proposed IsaR1 regulon depicted in Figure 7. Columns 1-5 contain a description of the potential targets (column 1: gene name; column 2: locus tag; column 3: operon structure of the proposed targets with regard to reference [S7]; column 4: description of gene function or functional category; column 5: information if the respective protein has iron (iron atom), heme or any kind of iron sulfur cluster (FeS) as cofactor). The remaining columns contain target prediction and experimental data as evidence for a regulation by IsaR1. Data fields which support a direct or indirect regulation are highlighted in green. Computational target prediction: A CopraRNA or IntaRNA prediction rank ≤100. Response to pulsed IsaR1 overexpression (microarray): Transcripts with an absolute log2-fold change of ≥0.9 and an adjusted p-value ≤0.05 between IsaR1OE and the control strain were taken as potential targets. If transcripts were within the top-100 list predicted by CopraRNA or IntaRNA, we lowered the log2-fold change threshold to 0.5. Response to pulsed IsaR1 overexpression (SRM): Proteins with absolute log2-fold changes ≥0.8 were taken as potential targets. Response to pulsed IsaR1 overexpression (Western blot): A reduction of the protein amount of to ≤60% of the amount in the control strain. Response to iron depletion in the ΔIsaR1 strain (microarray): Transcripts with an absolute log2-fold change of ≥1.0 and an adjusted p-value ≤0.05 were taken as

potential targets. GFP-reporter assay: An at least 1.5 fold reduction of the GFP fluorescence.

Data S1. Whole genome expression plot showing an iron stress time course experiment for the WT and the Δ*isaR1* mutant. Related to **Figure 2**. The iron-specific chelator DFB was added to cultures at iron-replete conditions (T = 0h) and then samples were taken at the indicated time points for 3 consecutive days. Both strands of the respective chromosomal regions are shown with the location of annotated (protein coding) genes (blue boxes), antisense RNAs (red), and intergenic sRNA genes (yellow). Signals derived from individual microarray probes are represented by black to green (WT) and red (Δ*isaR1*) horizontal bars, respectively and the time course is indicated by the color gradient. The read numbers for primary transcripts (right y-axis) from a differential RNAseq experiment after 24 h of iron starvation (orange-grey) or exponentially growing cells (blue-grey) were taken from Kopf et al. [S7]. The scale for the microarray data is given at the left y-axis in $\log_2$ scale. All probes of a single RNA feature are connected by lines. The raw data for WT were taken from [S8] but differently normalized.

Data S2. Microarray and target prediction data. Related to **Figure 2A, Figure 3A** and **Figure 4.** Data sheet 1. Microarray data for the iron stress time course experiment with *Synechocystis* 6803 WT and the Δ*isaR1* mutant. The table displays $\log_2$ fold changes in transcript abundancies in the iron stress time course experiment (see **Data S1**). Features are separated into mRNAs, antisense RNAs (asRNAs), non-coding sRNAs (sRNAs), 5'UTRs and transcripts derived from internal (within CDS) TSSs (int). Fold changes were regarded as significant when the absolute $\log_2$ value was ≥1 and the corresponding adjusted p-value ≤0.05.

Data sheet 2. Microarray data for the *Synechocystis* 6803 IsaR1 pulsed overexpression experiment. The table displays $\log_2$ fold changes in transcript

abundancies (see **Data S3**). Features are separated into mRNAs, antisense RNAs (asRNAs), non-coding sRNAs (sRNAs), 5'UTRs and transcripts derived from internal (within CDS) TSSs (int). Transcripts with an absolute log_2 fold change of ≥0.9 and an adjusted p-value ≤0.05 between IsaR1OE and the control strain 6h after induction of IsaR1 expression were taken as potential targets. Additionally, the transcripts which showed a significantly different response to the copper addition were included (i.e., |(IsaR1OE 6h – IsaR1OE 0h) – (WT_pVZ 6h – WT_pVZ 0h)| 0.9, adj. p-value ≤ 0.05) (Figure 4). Furthermore, we excluded all differentially expressed genes from time point 0h (IsaR1OE 0h – WT_pVZ 0h <0.8) to obtain only targets which responded to the IsaR1 overexpression. If transcripts were additionally within the top 100 list predicted by CopraRNA or IntaRNA, we lowered the log_2 fold change threshold to 0.5.

Data sheet 3. Whole genome IsaR1 target prediction using the CopraRNA algorithm [S5, S6]. The first sheet contains the p-value sorted CopraRNA prediction. First column: False discovery rate calculated after Benjamini Hochberg (fdr). Second column: CopraRNA p-value. Third column: Annotation of the homologous protein genes. 4th to 23rd column: Organism specific results following the scheme: locus_tag(Gene name|Intarna energy|IntaRNA p-value|start interaction target|end interaction target|start interaction IsaR1|end interaction IsaR1|Entrez GeneID), position 200 in the target corresponds to the respective first nucleotide of the annotated start codon. 24th column: Locus tags of additional homologs to the respective gene in *Synechocystis*. Only the best p-value of all homologs is considered in CopraRNA. 25th column: Number of sampled p-values for the respective homolog. If a homolog is not present in all 20 organisms the missing p-values are sampled based on a multivariate normal distribution.

Data sheet 4. Whole genome IsaR1 target prediction using the IntaRNA algorithm.

Data S3. Whole genome expression plot showing the pulsed overexpression of IsaR1 at iron replete conditions. Related to **Figure 4**. Overexpression of IsaR1 was triggered by the addition of $CuSO_4$ to a final concentration of 2 µM (**Figure S3**) and the same copper concentration was adjusted in the control culture (WT). The time point (T = 0h) was taken immediately prior to the addition of copper and the other samples after 6 h. Both strands of the respective chromosomal regions are shown with identical symbols and colors as in **Data S1**.

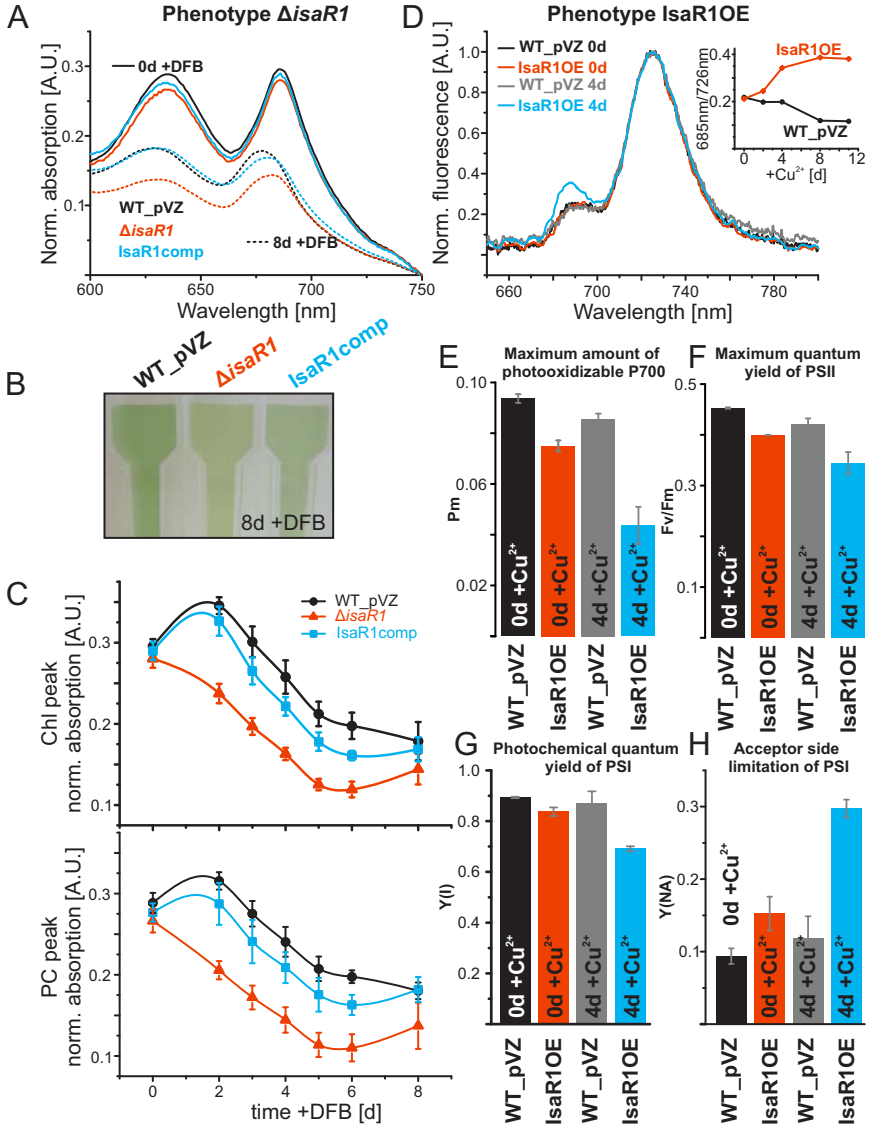
A
Phenotype ΔisaR1
Norm. absorption [A.U.]
0d +DFB
8d +DFB
WT_pVZ
ΔisaR1
IsaR1comp
Wavelength [nm]
D
Phenotype IsaR1OE
Norm. fluorescence [A.U.]
WT_pVZ 0d
IsaR1OE 0d
WT_pVZ 4d
IsaR1OE 4d
685nm/726nm
IsaR1OE
WT_pVZ
+Cu2+ [d]
Wavelength [nm]
B
WT_pVZ
ΔisaR1
IsaR1comp
8d +DFB
C
Chl peak norm. absorption [A.U.]
PC peak norm. absorption [A.U.]
WT_pVZ
ΔisaR1
IsaR1comp
time +DFB [d]
E
Maximum amount of photooxidizable P700
Pm
F
Maximum quantum yield of PSII
Fv/Fm
G
Photochemical quantum yield of PSI
Y(I)
H
Acceptor side limitation of PSI
Y(NA)
0d +Cu2+
4d +Cu2+
WT_pVZ
IsaR1OE

higher in WT ⟵ ⟶ higher in Δ*isaR1*

A

B

$-\log_{10}$ (adjusted p−Value)

0h DFB

48h DFB

$\Delta isaR1$ - WT

IsaR1
gifA
frpC
pilA11
gifB
slr1704
pilA9
slr0967
slr2018
pilA10
ssr2848
ssr1038
ssr1528
norB
sll0550
ndhD3
cupA
cccS
slr1513
cmpC
flv4
cmpB
sbtA
sll1735
sll0218
slr0042
ndhJ
IsiR
ndhI
ndhB
ndhG
flv2
ndhF3
slr0616
cccP
slr0476
cmpA
ndhC
slr0006
cmpD
cph1
nrtA
nirA
cyp
bicA
nrtC
glnA
nrtB
amt1
urtA
atpB
hliA
frp
cupB
psbI
cynS
IsaR1
kpsM
slr0108
slr0355
petF
ssr3570
ssr3571
ssr3572
psbZ
ycf35
atpI
sll1348
slr0551
ssl1263
slr0109
kpsT
sodB
atp1
Norf7
acnB
sufS
atpH
rbcS
sufD
cpcB
atpG
sll1696
hliB
cpcG2
sufC
atpA
atpF
psaJ
sll1240
cpcC1
cpcA
slr7076
cpcD
psbO
atpD
psaF
atpC
notB
cpcC2
psaK1
cccS
psaM
slr1544
apcB
hliC
apcA
hliA
ATP synthesis coupled proton transport
Photosystem I
NADH dehydrogenase activity
Nitrate assimilation
Phycobilisome
Photosystem II
Transposition
CO_2 assimilation / stress associated
Motilitiy / phototaxis
High light inducible proteins
Iron sulfur cluster biogenesis

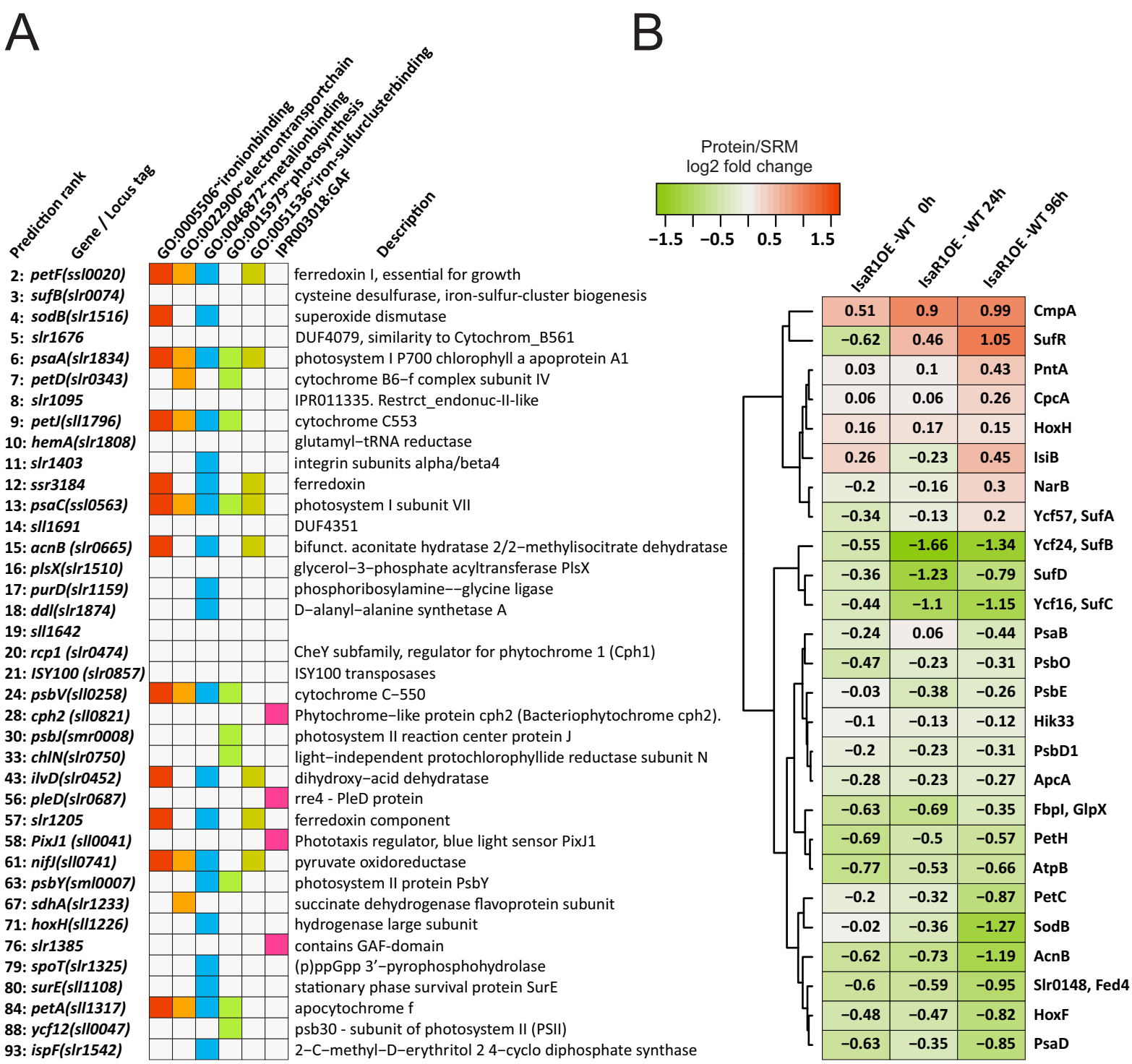
A
B
Prediction rank
Gene / Locus tag
GO:0005506~ironionbinding
GO:0022900~electrontransportchain
GO:0046872~metalionbinding
GO:0015979~photosynthesis
GO:0051536~iron-sulfurclusterbinding
IPR003018:GAF
Description
2: petF(ssl0020) ferredoxin I, essential for growth
3: sufB(slr0074) cysteine desulfurase, iron-sulfur-cluster biogenesis
4: sodB(slr1516) superoxide dismutase
5: slr1676 DUF4079, similarity to Cytochrom_B561
6: psaA(slr1834) photosystem I P700 chlorophyll a apoprotein A1
7: petD(slr0343) cytochrome B6−f complex subunit IV
8: slr1095 IPR011335. Restrct_endonuc-II-like
9: petJ(sll1796) cytochrome C553
10: hemA(slr1808) glutamyl−tRNA reductase
11: slr1403 integrin subunits alpha/beta4
12: ssr3184 ferredoxin
13: psaC(ssl0563) photosystem I subunit VII
14: sll1691 DUF4351
15: acnB (slr0665) bifunct. aconitate hydratase 2/2−methylisocitrate dehydratase
16: plsX(slr1510) glycerol−3−phosphate acyltransferase PlsX
17: purD(slr1159) phosphoribosylamine−−glycine ligase
18: ddl(slr1874) D−alanyl−alanine synthetase A
19: sll1642
20: rcp1 (slr0474) CheY subfamily, regulator for phytochrome 1 (Cph1)
21: ISY100 (slr0857) ISY100 transposases
24: psbV(sll0258) cytochrome C−550
28: cph2 (sll0821) Phytochrome−like protein cph2 (Bacteriophytochrome cph2).
30: psbJ(smr0008) photosystem II reaction center protein J
33: chlN(slr0750) light−independent protochlorophyllide reductase subunit N
43: ilvD(slr0452) dihydroxy−acid dehydratase
56: pleD(slr0687) rre4 - PleD protein
57: slr1205 ferredoxin component
58: PixJ1 (sll0041) Phototaxis regulator, blue light sensor PixJ1
61: nifJ(sll0741) pyruvate oxidoreductase
63: psbY(sml0007) photosystem II protein PsbY
67: sdhA(slr1233) succinate dehydrogenase flavoprotein subunit
71: hoxH(sll1226) hydrogenase large subunit
76: slr1385 contains GAF-domain
79: spoT(slr1325) (p)ppGpp 3'−pyrophosphohydrolase
80: surE(sll1108) stationary phase survival protein SurE
84: petA(sll1317) apocytochrome f
88: ycf12(sll0047) psb30 - subunit of photosystem II (PSII)
93: ispF(slr1542) 2−C−methyl−D−erythritol 2 4−cyclo diphosphate synthase
Protein/SRM
log2 fold change
−1.5 −0.5 0.5 1.5
IsaR1OE -WT 0h
IsaR1OE - WT 24h
IsaR1OE -WT 96h
0.51 0.9 0.99 CmpA
−0.62 0.46 1.05 SufR
0.03 0.1 0.43 PntA
0.06 0.06 0.26 CpcA
0.16 0.17 0.15 HoxH
0.26 −0.23 0.45 IsiB
−0.2 −0.16 0.3 NarB
−0.34 −0.13 0.2 Ycf57, SufA
−0.55 −1.66 −1.34 Ycf24, SufB
−0.36 −1.23 −0.79 SufD
−0.44 −1.1 −1.15 Ycf16, SufC
−0.24 0.06 −0.44 PsaB
−0.47 −0.23 −0.31 PsbO
−0.03 −0.38 −0.26 PsbE
−0.1 −0.13 −0.12 Hik33
−0.2 −0.23 −0.31 PsbD1
−0.28 −0.23 −0.27 ApcA
−0.63 −0.69 −0.35 FbpI, GlpX
−0.69 −0.5 −0.57 PetH
−0.77 −0.53 −0.66 AtpB
−0.2 −0.32 −0.87 PetC
−0.02 −0.36 −1.27 SodB
−0.62 −0.73 −1.19 AcnB
−0.6 −0.59 −0.95 Slr0148, Fed4
−0.48 −0.47 −0.82 HoxF
−0.63 −0.35 −0.85 PsaD

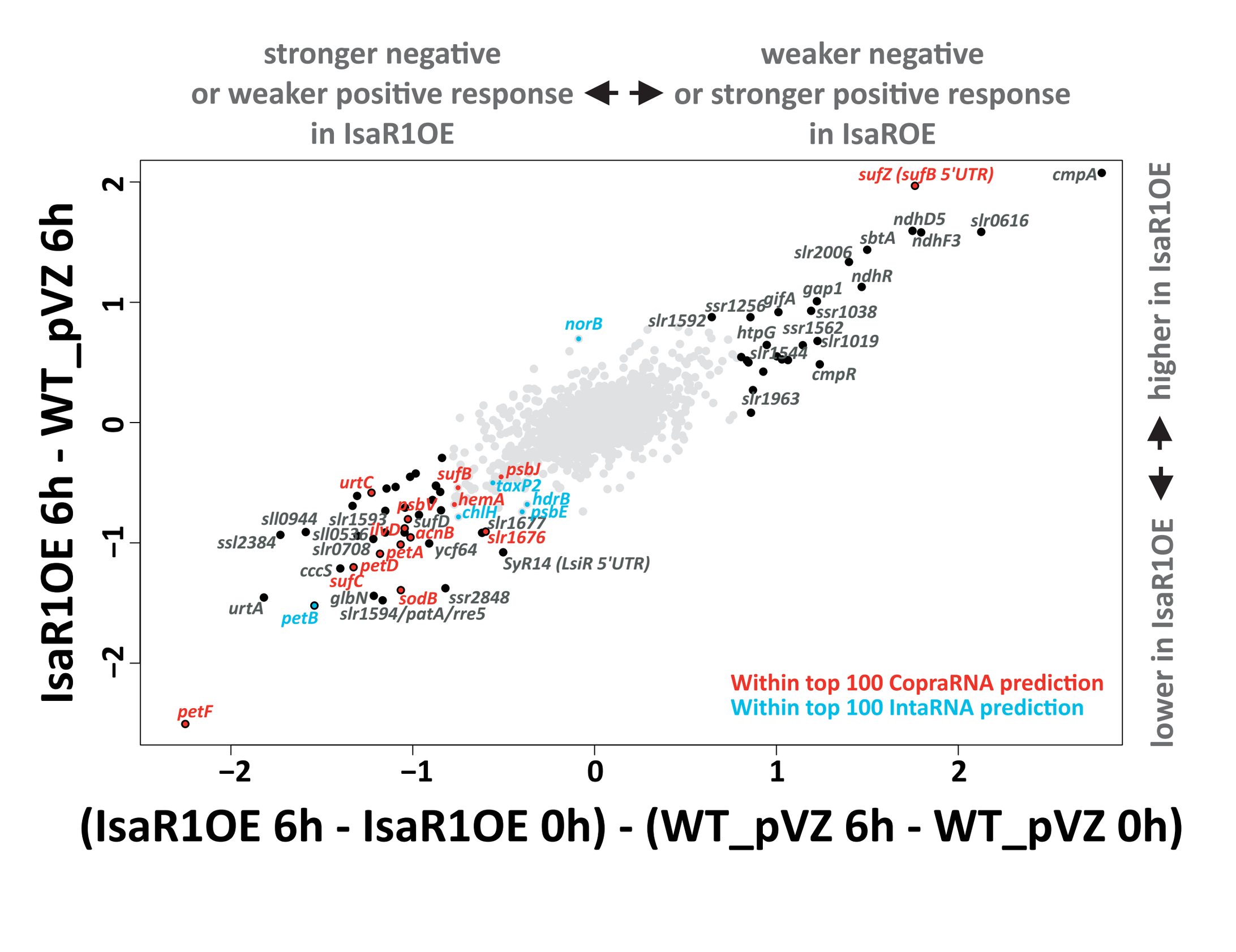
stronger negative
or weaker positive response
in IsaR1OE
weaker negative
or stronger positive response
in IsaROE
IsaR1OE 6h - WT_pVZ 6h
(IsaR1OE 6h - IsaR1OE 0h) - (WT_pVZ 6h - WT_pVZ 0h)
lower in IsaR1OE ← → higher in IsaR1OE
sufZ (sufB 5'UTR)
cmpA
ndhD5
slr0616
sbtA
ndhF3
slr2006
ndhR
gap1
gifA
ssr1256
ssr1038
slr1592
norB
htpG
ssr1562
slr1019
slr1544
cmpR
slr1963
psbJ
sufB
urtC
taxP2
hemA
hdrB
psbV
chlH
psbE
sll0944
slr1593
sufD
slr1677
ssl2384
sll0536
ilvD
acnB
slr1676
slr0708
petA
ycf64
SyR14 (LsiR 5'UTR)
cccS
petD
sufC
glbN
sodB
ssr2848
urtA
petB
slr1594/patA/rre5
petF
Within top 100 CopraRNA prediction
Within top 100 IntaRNA prediction
−2
−1
0
1
2

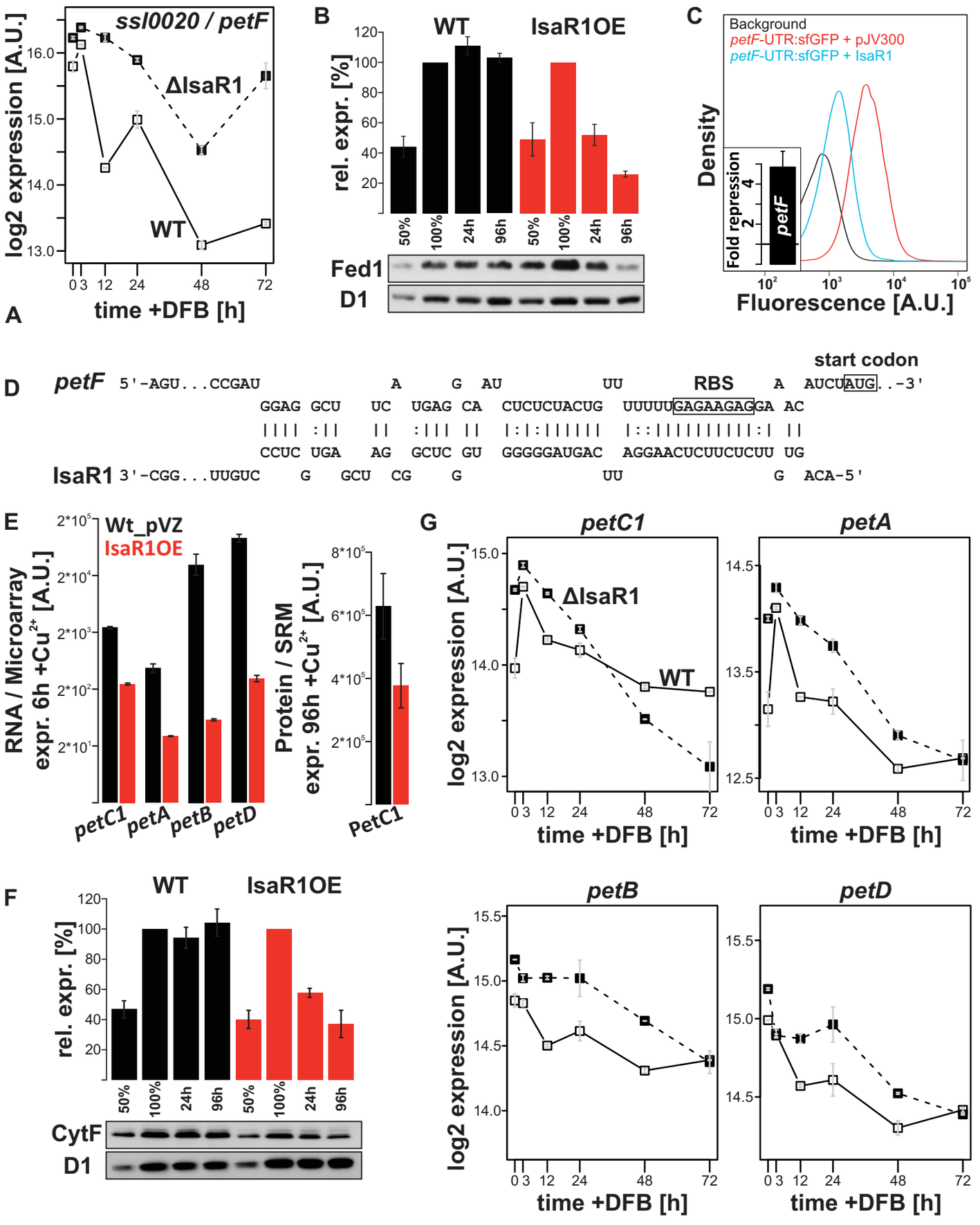
A
ssl0020 / petF
ΔIsaR1
WT
log2 expression [A.U.]
time +DFB [h]
B
WT
IsaR1OE
rel. expr. [%]
50%
100%
24h
96h
Fed1
D1
C
Background
petF-UTR:sfGFP + pJV300
petF-UTR:sfGFP + IsaR1
Density
Fold repression
petF
Fluorescence [A.U.]
D
petF 5'-AGU...CCGAU
start codon
RBS
AUCUAUG..-3'
IsaR1 3'-CGG...UUGUC
ACA-5'
E
Wt_pVZ
IsaR1OE
RNA / Microarray expr. 6h +Cu2+ [A.U.]
Protein / SRM expr. 96h +Cu2+ [A.U.]
petC1
petA
petB
petD
PetC1
F
WT
IsaR1OE
rel. expr. [%]
CytF
D1
G
petC1
petA
petB
petD
ΔIsaR1
WT
log2 expression [A.U.]
time +DFB [h]

Figure 5

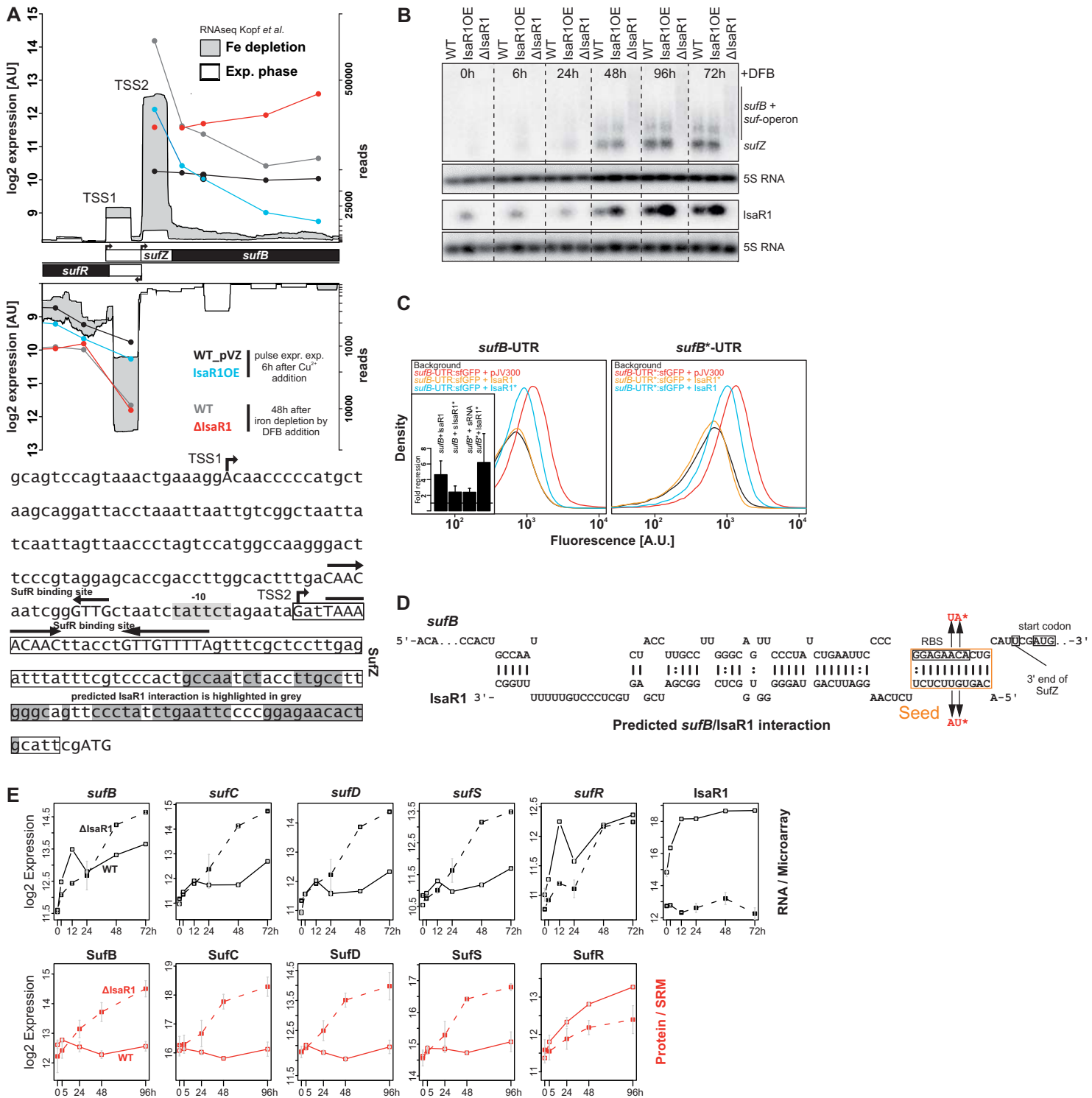
A
RNAseq Kopf et al.
Fe depletion
Exp. phase
TSS2
TSS1
log2 expression [AU]
reads
sufZ
sufB
sufR
WT_pVZ
IsaR1OE
pulse expr. exp. 6h after Cu2+ addition
WT
ΔIsaR1
48h after iron depletion by DFB addition
gcagtccagtaaactgaaaggACaaccccccatgct
aagcaggattacctaaattaattgtcggctaatta
tcaattagttaaccctagtccatggccaagggact
tcccgtaggagcaccgaccttggcactttgaCAAC
SufR binding site
-10
TSS2
aatcggGTTGctaatctattctagaataGatTAAA
SufR binding site
ACAACttacctGTTGTTTTAgtttcgctccttgag
SufZ
atttatttcgtcccactgccaatctaccttgcctt
predicted IsaR1 interaction is highlighted in grey
gggcagttccctatctgaattcccggagaacact
gcattcgATG
B
WT
IsaR1OE
ΔIsaR1
0h
6h
24h
48h
96h
72h
+DFB
sufB + suf-operon
sufZ
5S RNA
IsaR1
C
sufB-UTR
sufB*-UTR
Background
sufB-UTR:sfGFP + pJV300
sufB-UTR:sfGFP + IsaR1
sufB-UTR:sfGFP + IsaR1*
sufB*-UTR*:sfGFP + pJV300
sufB*-UTR*:sfGFP + IsaR1*
sufB*-UTR*:sfGFP + IsaR1
Density
Fold repression
sufB+ IsaR1
sufB + sIsaR1*
sufB* + sRNA
sufB*+ IsaR1*
Fluorescence [A.U.]
D
sufB
5'-ACA...CCACU U ACC UU A UU U CCC RBS CAUUCGAUG..-3'
GCCAA CU UUGCC GGGC G CCCUA CUGAAUUC GGAGAACACUG
CGGUU GA AGCGG CUCG U GGGAU GACUUAGG UCUCUUGUGAC
IsaR1 3'- UUUUUGUCCCUCGU GCU G GG AACUCU A-5'
UA*
AU*
Seed
start codon
3' end of SufZ
Predicted sufB/IsaR1 interaction
E
sufB
sufC
sufD
sufS
sufR
IsaR1
ΔIsaR1
WT
log2 Expression
RNA / Microarray
SufB
SufC
SufD
SufS
SufR
Protein / SRM

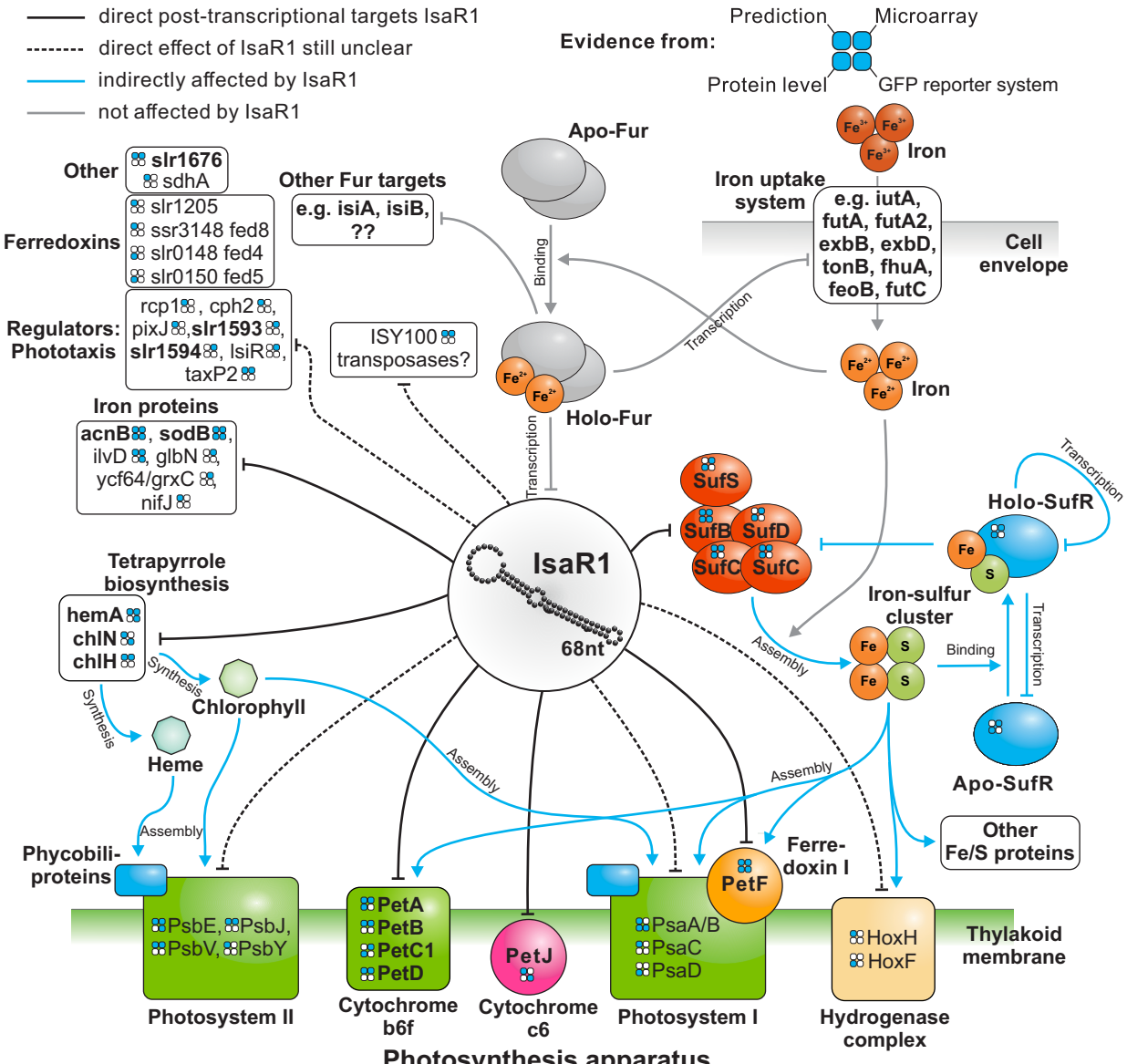
direct post-transcriptional targets IsaR1
direct effect of IsaR1 still unclear
indirectly affected by IsaR1
not affected by IsaR1
Evidence from:
Prediction
Microarray
Protein level
GFP reporter system
Iron
Iron uptake system
e.g. iutA, futA, futA2, exbB, exbD, tonB, fhuA, feoB, futC
Cell envelope
Apo-Fur
Binding
Other
slr1676
sdhA
Other Fur targets
e.g. isiA, isiB, ??
Ferredoxins
slr1205
ssr3148 fed8
slr0148 fed4
slr0150 fed5
Regulators: Phototaxis
rcp1, cph2, pixJ, slr1593, slr1594, lsiR, taxP2
ISY100 transposases?
Transcription
Holo-Fur
Iron proteins
acnB, sodB, ilvD, glbN, ycf64/grxC, nifJ
IsaR1
68nt
SufS
SufB
SufD
SufC
SufC
Holo-SufR
Apo-SufR
Iron-sulfur cluster
Assembly
Binding
Tetrapyrrole biosynthesis
hemA
chlN
chlH
Synthesis
Chlorophyll
Heme
Phycobili-proteins
PsbE, PsbJ, PsbV, PsbY
Photosystem II
PetA
PetB
PetC1
PetD
Cytochrome b6f
PetJ
Cytochrome c6
PetF
Ferre-doxin I
PsaA/B
PsaC
PsaD
Photosystem I
HoxH
HoxF
Hydrogenase complex
Other Fe/S proteins
Thylakoid membrane
Photosynthesis apparatus